Accepted Manuscript

Sedimentology of the ~3.3 Ga upper Mendon Formation, Barberton Greenstone Belt, South Africa

Elizabeth J. Trower, Donald R. Lowe

PII: S0301-9268(16)30187-5
DOI: http://dx.doi.org/10.1016/j.precamres.2016.06.003
Reference: PRECAM 4524

To appear in: *Precambrian Research*

Received Date: 29 November 2015
Revised Date: 25 May 2016
Accepted Date: 4 June 2016

Please cite this article as: E.J. Trower, D.R. Lowe, Sedimentology of the ~3.3 Ga upper Mendon Formation, Barberton Greenstone Belt, South Africa, *Precambrian Research* (2016), doi: http://dx.doi.org/10.1016/j.precamres.2016.06.003

Sedimentology of the ~3.3 Ga upper Mendon Formation, Barberton Greenstone Belt, South Africa

Elizabeth J. Trower[1]* and Donald R. Lowe[2]

[1]Division of Geological and Planetary Sciences, California Institute of Technology, Pasadena, CA 91125, USA

[2]Department of Geological and Environmental Sciences, Stanford University, Stanford, CA 94305, USA

*Corresponding author: ltrower@caltech.edu

Abstract

The Mendon Formation is the uppermost unit of the 3.5-3.26 Ga Onverwacht Group in the Barberton Greenstone Belt, South Africa. It consists of a cyclic stack of komatiitic volcanic units separated by thin cherty sedimentary layers. In most areas, the uppermost Mendon Formation is a sedimentary interval characterized by black chert, banded black-and-white chert, and banded ferruginous chert, although the detailed patterns of lithofacies in different sections are more complex. Previously reported zircon U/Pb ages suggest that Mendon deposition could represent more than 70 Myr of time between ~3,334 Ma and ~3,260 Ma.

This study presents sedimentological and petrographic observations of the upper Mendon Formation from across the central part of the Barberton Greenstone Belt in order to investigate sediment sources, depositional processes, and environments of sedimentation. The dominant mode of sedimentation was quiet settling of carbonaceous grains and, in the deepest sections below storm wave base, fine ferruginous material, resulting in finely laminated black and grey chert. *In situ* carbonaceous laminations are rare, suggesting that benthic microbial mat growth had little direct influence on deposition. The hemipelagic background deposition was punctuated by occasional inputs of fine pyroclastic debris, formation and deposition of silica granules, and reworking by infrequent storm

events. Storm deposits are represented by coarse-grained, poorly-sorted intraclast breccias, some of which include distinctive intraclasts sampling lithofacies that are not observed *in situ*. Despite considerable lateral variability, correlative temporal trends are resolvable in many Mendon sections: there is an upward-deepening of the overall depositional setting recorded in the oldest upper Mendon sections, consistent with the previous interpretation that Mendon time was characterized by rifting (Lowe, 1994a; Lowe, 1999a). Younger Mendon cycles include thick, relatively ferruginous basal sections, interpreted to reflect the deepest water deposition. These sections are capped by black chert and silicified ashes with more evidence of disturbance and reworking by storms, reflecting gradual shoaling. This sedimentological analysis is broadly consistent with previous geochemical and tectonic analyses and provides a better picture of depositional patterns during uppermost Onverwacht time, before the distinct change in tectonic regime marked by impact spherule layer S2 and the onset of Fig Tree Group orogenesis and related siliciclastic deposition.

Keywords: Mendon Formation; Barberton Greenstone Belt; chert; sedimentology; petrography; Archean

1. Introduction

The 3.5-3.3 Ga Onverwacht Group in the Barberton Greenstone Belt, South Africa, is a prime example of non-uniformitarianism in Archean geology. There is no Phanerozoic equivalent to this thick succession of basalts, komatiites, and thin sedimentary chert units that spans ~270 Myr (Armstrong et al., 1990; Byerly et al., 1996; Lowe and Byerly, 1999). The sedimentary rocks present a particular challenge because they lack the components that are central to many sedimentological analyses: they are neither classic siliciclastic nor carbonate rocks, the dominant sedimentological modes of the post-Archean sedimentary record. At least locally, there was little continental crust to provide detrital sedimentary material and the dominantly mafic and ultramafic volcanism yielded few sand-sized detrital

grains upon weathering (Lowe, 1999b). Pyroclastic fall deposits and reworked volcaniclastic sandstones occur, but many lithofacies are not clearly volcanic in origin, including black chert, banded black-and-white chert, and banded ferruginous chert (Lowe, 1999c; Lowe and Byerly, 1999). Many of these rocks have extremely low alumina contents (<1 wt. %) and are composed of carbonaceous grains and/or laminations, fine ferruginous material (commonly siderite when unweathered), and silica in the form of microquartz (Lowe, 1999b; Walsh and Lowe, 1999). The origins of each of these components is problematic: is the carbonaceous material biogenic? If so, can it be used to provide insights into the early Archean biosphere? What was the original mineralogy of the iron and was it associated with iron-based microbial metabolic activity? How much of the silica is diagenetic versus primary? Were all cherts formed via silicification adjacent to hydrothermal vents (Paris et al., 1985), or was silica precipitation a more widespread primary (Stefurak et al., 2014; Stefurak et al., 2015) and early diagenetic process due to high silica concentrations in seawater (Siever, 1992; Maliva et al., 2005)? This study applies a sedimentological approach to understanding the complex interplay of carbonaceous, ferruginous, siliceous, and volcanic inputs in the upper Mendon Formation, a ~50-m-thick ~3.3 Ga sedimentary chert unit capping the Onverwacht Group. Despite being interpreted as a relatively quiet, deep water deposit (Lowe and Byerly, 1999), there is considerable lithologic variability among sections of the upper Mendon Formation across different segments of the Barberton Greenstone Belt, providing a possible means for distinguishing local vs. regional differences in sediment sources, depositional processes, and depositional environments.

2. Geologic background

The Barberton Greenstone Belt (BGB) is a heavily deformed 3.5-3.2 Ga volcano-sedimentary terrain in South Africa and northern Swaziland (Fig. 1). The basal unit in the BGB is the Onverwacht Group, an 8-10 km thick sequence of largely mafic and ultramafic volcanic rocks with thin intervening

sedimentary cherts representing periods of volcanic quiescence (Lowe and Byerly, 1999). The overlying Fig Tree Group comprises a variety of volcaniclastic, terrigenous, and chemical sedimentary rocks that reflect a major change in tectonic style – the onset of orogenesis (Lowe, 1999a; Lowe and Byerly, 1999; Lowe and Nocita, 1999). The Mendon Formation is the uppermost unit of the Onverwacht Group. Because of deformation and faulting, the Mendon Formation, and particularly the upper cherty Mendon Formation, crops out widely in a series of folds and fault-bounded structural belts across the BGB (Lowe and Byerly, 1999) (Fig. 2).

Previous studies have identified at least 5 cycles of volcanism and sedimentation in the Mendon Formation, manifested as alternating layers of komatiitic volcanic rocks, termed from base upward M1v, M2v, M3v, M4v, and M5v, and thin intervening sedimentary units, M1c, M2c, M3c, M4c, and M5c. The sedimentary layers are now composed largely of silicified volcaniclastic sediments, black chert, banded black-and-white chert, and banded ferruginous chert (Byerly, 1999; Lowe and Byerly, 1999; Decker et al., 2015). This stratigraphy is complicated by the observation that most Mendon sections do not contain the full sequence of volcanic cycles. Previous authors have suggested that this is related to diachronous onset and conclusion of upper Mendon deposition across different structural belts in the BGB related to contemporaneous rifting (Fig. 2) and/or that local topographic highs impeded the lateral continuity of volcanic units (Lowe, 1994a; Byerly, 1999; Lowe, 1999a; Lowe and Byerly, 1999; Thompson Stiegler et al., 2010; Decker et al., 2015).

The age of the Mendon Formation is constrained by a maximum age of 3,334 ± 3 Ma from a zircon U/Pb age in a tuffaceous band in the uppermost Kromberg Formation (Byerly et al., 1996) and a minimum age of ~3,260 Ma, based on two ages from tuffs in the base of the overlying Mapepe Formation: 3,259 ± 4 Ma (Byerly et al., 1996) and 3267 ± 7 Ma (Decker et al., 2015). Several zircon U/Pb ages have also been reported from units within the Mendon Formation: 3,298 ± 3 Ma from a thin tuffaceous layer in M3c (Byerly et al., 1996), 3,287 ± 3 Ma from a felsic ash in M2c near the Swaziland

border (Decker et al., 2015), and 3,280 ± 9 Ma from a tuffaceous sandstone above M4c in the Barite Syncline locality (see sample locations BS-02 and BS-03 in Fig. 2) (Decker et al., 2015). The depositional rates of the rapidly erupted komatiites were probably enormously greater than those of the interbedded fine-grained carbonaceous, siliceous, and ferruginous sediments, implying that the sedimentary lithofacies of the upper Mendon Formation represent the majority of the accumulation time recorded: up to 75 million years, but potentially somewhat less time considering that there may be unconformities within the sequence.

The uppermost 50-70 m of the Mendon Formation (referred to hereafter as the upper Mendon Formation) are in most areas composed of interlayered black chert (laminated or massive), grey-weathering chert (laminated or massive), banded black-and-white chert, banded ferruginous chert, and silicified ash beds. Despite the overall low energy depositional setting of the upper Mendon Formation (Lowe and Byerly, 1999), we observe a considerable degree of vertical and lateral lithologic variability. This variability likely results from a combination of factors, including: 1) variations in the primary sediment input, 2) proximity to sites of eruption and distribution of volcaniclastic materials, and 3) environment-related variations in chemical sedimentation. In this paper, we explore some of this variability and evaluate its potential causes.

3. Methods

This study incorporates measured stratigraphic sections, thin section petrography, and geochemistry to characterize and compare rocks of the upper Mendon Formation in the southern domain of the BGB. Twelve stratigraphic sections were measured in various structural belts within the southern domain of the BGB (Fig. 2, Supp. Table S1). A total of 244 samples were collected for slabbing and/or thin-sectioning. A total of 185 thin sections representing the measured sections were analyzed to identify major grain types. The grain compositions of 29 intraclast breccia beds were point counted in

order to compare and contrast these more energetic deposits among different sections. Point counting was carried out using PETROG wireless stepping counting stage and PetrogLite point counting software, with 400 points per sample, including matrix/cement. Grain classifications are summarized in Supp. Table S2.

This study includes data from thirteen samples sent to the Washington State University GeoAnalytical Lab for analyses of major, trace, and rare earth element (REE) abundances using a Thermo-ARL automated X-ray fluorescence spectrometer (XRF) and an Agilent inductively coupled plasma mass spectrometer (ICP-MS). These analyses are supplemented with selected geochemical data presented by Walsh (1989) and Lowe (1999b) (see Supp. Table S3).

Raman spectra were collected from polished thin sections using a Renishaw RM1000 Raman microscope in the Extreme Environments Laboratory at Stanford University using a 514 nm laser oriented normal to the sample, with spatial resolution of up to 1 µm. Spectra were compared to the RRUFF database of known reference materials (Downs, 2006).

4. Lithofacies of the upper Mendon Formation

4.1. Black chert

This lithofacies is black, gray, or slightly earthy brown in outcrop and black on fresh surfaces, finely laminated (Fig. 3a), and typically composed of fine-grained carbonaceous material in a matrix of microquartz, with volcanic material (e.g. ash and accretionary lapilli) and silica granules as common but quantitatively minor accessory components. Some black chert contains thin (1-3 cm thick) graded beds dominated by white- to light grey-weathering ash-rich material at the bases and grading into dark, dominantly carbonaceous material at the tops (Fig. 3c). We interpret that each graded bed represents an individual fall deposit from a relatively distant pyroclastic eruption (Thompson Stiegler et al., 2011). Current structures (e.g. ripple cross-lamination, see Fig. 3b) are rarely observed and typically associated

with the presence of fine ash-rich material. The fine-grained, finely laminated nature of black chert indicates quiet water sedimentation, likely below storm wave base.

4.2. Grey chert

The main distinction between grey and black chert is compositional – a lower content of carbonaceous matter and a greater content of iron-bearing materials – resulting in grey to slightly reddish color on weathered surfaces. Grey chert is typically finely laminated and composed of very fine grained carbonaceous matter, ferruginous material including goethite, and, in unweathered samples or core, siderite and a minor component of phyllosilicates (Fig. 3d). Current structures are not observed in grey chert; based on this and the finer grain size compared with black chert, we interpret that grey chert was deposited in quieter and likely deeper settings than black chert.

4.3. Banded black-and-white chert

Banded black and white chert (BBWC) is characterized by alternating cm-scale bands of relatively pure white-weathering, translucent chert and laminated or massive fine-grained black chert. Both layer types are tabular and typically laterally continuous at scales of several meters, although local brecciation of white chert bands is common (Fig. 3e). Current structures, such as ripple cross-lamination, are generally absent from both types of bands in BBWC. Thin (most >2 cm thick) stratiform void-filling cements composed of coarse megaquartz and botryoidally layered chert commonly occur immediately below white bands in banded black and white chert. Stefurak et al. (2014; 2015) recognized that many white bands were originally sedimentary layers composed of silica granules, primary sub-spherical sand-sized chemical sand grains originally composed of amorphous silica. Although silica granules are not readily apparent in all black-and-white banded chert in the Mendon Formation, white bands are morphologically identical at a macro-scale regardless of whether silica granules are visible in outcrop or thin section and we consider it likely that most, if not all, white chert bands were deposited as layers of relatively pure silica granules. The BBWC of the Mendon Formation is comparable to the upper BBWC

facies of the Buck Reef Chert in the basal Kromberg Formation, which is interpreted as having been deposited in a lower energy depositional environment at or below storm wave base (>200 m) (Tice and Lowe, 2006). Brecciation of white chert bands suggests that BBWC experienced episodic influence by storm currents.

4.4. Banded ferruginous chert

Banded ferruginous chert (BFC) is similar to BBWC but characterized by alternating white or slightly pinkish relatively pure chert bands and layers of laminated ferruginous chert. In general, the thicknesses of bands in BFC are less than those in BBWC and brecciation of white chert bands is less common. Compositionally, there is a relatively continuous gradation between BBWC and BFC. Laminated ferruginous layers commonly display small-scale load structures (several cm wide) into underlying white chert layers (Fig. 3f), likely related to a strong initial density contrast between the ferruginous material and the underlying amorphous silica layer. We interpret that BFC represents deeper-water sedimentation than BBWC due to the less frequent occurrence of chert plate breccias and its finer-grained and more finely banded nature. This interpretation is consistent with the conclusions of previous authors that lithofacies with more iron-rich compositions, such as BFC, were deposited in basinal settings (Lowe and Byerly, 1999; Tice and Lowe, 2006).

4.5. Intraclast breccias

Intraclast breccia layers, typically 5-30 cm thick, occur in most upper Mendon sequences. These layers are particularly noticeable given the general paucity of current structures or coarse-grained deposits in the upper Mendon Formation. In contrast with other lithofacies described here, intraclast breccia layers typically have irregular or lenticular shapes and erosive lower contacts. Many intraclast breccias contain large white chert plates that are a few mm to several cm thick and 5-30 cm in length. In some cases, referred to here as Type 1 breccias, breccia layers can be traced laterally into intact BBWC

and the dominant clasts in the breccia are white chert plates. Type 1 breccias probably resulted from storm-related currents breaking and locally re-sedimenting brittle white chert hardgrounds.

In other cases, referred to here as Type 2 breccias, the breccia layers are more laterally extensive: for example, one distinctive breccia unit is observed at the same stratigraphic level in stratigraphic sections measured from tens to hundreds of meters apart in the Barite Syncline locality (Fig. 4). This layer contains two distinct types of clasts: extremely thin chert plates (>1 cm thick but commonly ≥5 cm in length) and coarse, well-rounded black chert intraclasts (Fig. 5). The matrix to these clasts is a now-silicified medium- to coarse-grained carbonaceous, volcaniclastic, and siliceous sandstone. The breccia unit occurs within finely laminated black chert and cm-scale graded beds of fine ash and carbonaceous material. Overall, the breccia layers are poorly- to very-poorly-sorted and loosely packed. The thin chert plates are commonly imbricated, although an individual breccia layer can display opposing directions of imbrication, consistent with oscillatory current reversals (Massari and D'Alessandro, 2000; Cantalamessa and Di Celma, 2005; Fujino et al., 2006). We interpret that Type 2 breccias were associated with higher energy and more prolonged current activity, related to larger storms and/or perhaps tsunamis (cf. Table 1 in Dawson and Stewart, 2007).

4.6. Silicified ash and accretionary lapilli

Silicified light grey to slightly greenish ash layers or beds of accretionary lapilli are a minor component of most upper Mendon Formation sections (Fig. 3g). Accretionary lapilli beds are normally graded, from granule-sized lapilli to very fine ash. Ash layers are fine-grained and flat-laminated or massive, with rare occurrences of cross-lamination (Fig. 3g). Some distinctive ash layers can be correlated between sections measured hundreds of meters apart (Supp. Fig. S1). Normal grading in accretionary lapilli and ash beds reflects their likely origin as pyroclastic fall deposits (Lowe, 1999c), with local reworking by weak currents in an otherwise quiet water setting.

5. General stratigraphy

The upper Mendon Formation chert has previously been described as broadly similar across structural belts south of the Inyoka Fault (Fig. 2). In detail, however, there is a considerable amount of lithologic variability among sections, expressed as differences in the proportions of chert types (black vs. grey vs. ferruginous) and texture (massive vs. laminated vs. banded), combined with the presence or absence of distinguishing features like current structures, intraclast breccias, and ash layers.

The sections in the southern structural belt (Figs. 2 and 6, Supp. Figs. S2-S5) are broadly distinguishable from sections in the northeastern domain (Fig. 7, Supp. Figs. S1, S6-S8) by the occurrence of a greater proportion of banded chert and the absence of a thick basal section composed of more ferruginous lithologies – finely laminated slightly ferruginous grey chert and/or BFC. The southern sections include the contact between the black, grey, and ferruginous chert of the uppermost Mendon Formation and the underlying Msauli Chert (M1c), a distinctive 20-35-m-thick unit of silicified komatiitic ash and accretionary lapilli capping the oldest Mendon volcanic cycle (M1v). This contact is typically erosional and is overlain by a thin layer of conglomerate and volcaniclastic sands indicating reworking of the uppermost Msauli Chert, although regional correlations of individual accretionary beds (Lowe, 1999c) indicate that there has been no significant erosion and removal of the uppermost Msauli Chert. Sections SAF 187 and SAF 191 also include a distinctive marker unit in M2c, a layer of very coarse accretionary lapilli (Supp. Figs. S2 and S3) (Lowe and Byerly, 1999).

The sections from northeastern structural belts overlie stratigraphically higher volcanic cycles (see Fig. 7, Supp. Figs. S1, S6-S8) – M3v (sections SAF 521 and BHR-01), M4v (sections BS-02 and BS-03), and M5v (sections BM-1, SAF 620, and CQ-01) – and are therefore largely younger than much of the black chert in the southern domain sections, which predates M2c (Fig. 6). These sections share the broad overall characteristic of somewhat ferruginous chert (laminated slightly ferruginous grey chert or BFC) overlain by black chert (Fig. 7). In the Barite Syncline area, the contact between the Mendon

Formation and the overlying Mapepe Formation of the Fig Tree Group is defined by spherule bed S2 and commonly marked by the occurrence of barite as bladed crystal fans and heavy mineral sand. Several sections of the uppermost Mendon Formation in this area (sections BS-02 and BS-03, see Supp. Fig. S1) contain correlatable beds (Fig. 4), despite local disruptions of stratigraphy due to many black chert dikes (Lowe, 2013). Detailed correlations like these are not readily apparent between other sets of sections, likely because these sections are currently separated by several kilometers and were probably much further apart initially since rocks of the Onverwacht Group have been subjected to several episodes of deformation including faulting and tight folding (Lowe et al., 1999). Subtle local differences in sediment composition, water depth, current energy, and other environmental factors could therefore have strongly influenced the sediments on a bed scale and precluded the deposition and/or preservation of correlative units.

6. Petrography

6.1. Carbonaceous material

Carbonaceous material is visually abundant in the form of sedimentary grains, finely disseminated matrix material, *in situ* laminations, and as thin coatings around other grains, although it is a relatively trace component in terms of chemical composition. Walsh and Lowe (1999) reported total organic carbon (TOC) contents of 0.28 to 4.33% in a variety of black chert samples from the Mendon Formation. Raman spectra confirm that grains, laminations, and coatings identified petrographically as carbonaceous are composed of disordered carbonaceous material (Supp. Fig. S10), rather than polycrystalline graphite or some other mineral with a superficially similar appearance. Peak positions and ratios of D/G peak areas (mean ratio ~1.8) are consistent with chlorite-zone greenschist-grade metamorphism (Yui et al., 1996; Xie et al., 1997; Tice et al., 2004). Simple and composite grains as

defined here are equivalent to the simple and composite carbonaceous grains identified by Walsh and Lowe (1999) and Tice and Lowe (2006).

6.1.1. Simple grains

The simplest type of carbonaceous grain consists of relatively fine (mostly <200 μm), unstructured particles of carbonaceous matter that range from irregular in shape and aspect ratio to relatively equant and round (Fig. 8a). Simple grains commonly have rough, irregular edges and range in apparent composition from dark and densely carbonaceous to lighter in color and much less densely carbonaceous. These grains are commonly compacted when found in layers dominated by carbonaceous grains, but less compacted when occurring within deposits of more varied grain composition (e.g. intraclast breccias), reflecting differences in cementation timing.

6.1.2. Composite grains

A similarly common, but more internally complex type of carbonaceous grain is the composite grain, which has a clotted, irregular internal texture composed of three or more domains that in some cases resemble simple grains (Fig. 8b, Supp. Fig. S10). Domains are distinguished visibly as more densely carbonaceous zones. Composite grains are roughly equant to somewhat oblong (aspect ratios < 3) in shape with irregular and ragged edges similar to those observed in simple grains. These grains are typically coarser than simple grains, generally ranging from 200-1000 μm. Some grains are rimmed by isopachous silica cement (Supp. Fig. S10).

6.1.3. Laminated carbonaceous intraclasts

Coarse intraclasts of somewhat diffusely laminated, densely carbonaceous chert occur almost exclusively in Type 2 intraclast breccia beds that are poorly sorted, loosely packed, and essentially uncompacted (Fig. 8c-e, Supp. Fig. S11). These intraclasts are elongated parallel to the direction of laminations, with thicknesses ranging from 100-1000 μm and lengths ranging from 500 μm to several centimeters. Although some laminations are relatively even and planar, many have irregular

morphologies including small domal or columnar features and steep truncations draped by subsequent laminations (Supp. Fig. S11). Some intraclasts also include cements precipitated between laminations. Sericitic chert and in some cases accretionary lapilli are also associated with some laminated carbonaceous intraclasts (Fig. 8d). These were layers of volcanic-derived sediments (ash and accretionary lapilli) initially interbedded with the laminated carbonaceous material.

6.1.4. Black chert intraclasts

Another type of grain exclusively limited to Type 2 intraclast breccia layers is the black chert intraclast. These intraclasts are less densely carbonaceous than the laminated intraclasts and have distinctly different internal textures typical of many Onverwacht black cherts, defined by an irregular distribution of carbonaceous matter, with domains resembling simple grains. These intraclasts are distinct from composite grains in that they have more varied compositions, including silica grains and tuffaceous material and have relatively smooth edges that truncate internal domains (Fig. 11, Supp. Fig. S12). These intraclasts are typically quite coarse (>2 cm in diameter), range from roughly equant in shape to somewhat oblong (aspect ratios <3), and are subangular to well-rounded.

6.1.5. In situ carbonaceous laminations

In situ carbonaceous laminations are relatively rare in the upper Mendon Formation. Some features referred to by previous authors as anastomosing laminations (e.g. Klr laminations of Tice and Lowe, 2006) are here identified as carbonaceous matrix material (see section 6.1.6) within a compacted layer of primary silica granules (see section 6.3) as per Stefurak et al. (2014). Fine carbonaceous laminations (<5 µm thick) separated by thin chert layers (<10 µm thick) occur mostly associated with ferruginous lithofacies (grey chert and in some laminated ferruginous bands of BFC, see Supp. Fig. S13) and as rare rip-up clasts within intraclast breccias (Fig. 8g). Laminations may be even and roughly parallel, or show simple anastomosing and branching morphologies. These laminations are comparable to lamination types Klb and Klm of Tice and Lowe (2006) and “fine carbonaceous laminations” described

by Walsh and Lowe (1999), although roll-up structures are relatively uncommon within the upper Mendon Formation.

A unique but remarkable example of a slightly different type of carbonaceous lamination occurs near the top of an intraclast breccia layer located ~1.5 m above the Msauli Chert in the SAF 186 section (Fig. 2 and Supp. Fig. S4). This set of fine laminations drapes smoothly over irregular topography created by large carbonaceous and siliceous intraclasts (Fig. 9). Unlike the previously described laminations which are separated by layers of relatively pure microquartz, these appear to trap silt- to fine-sand-sized particles between laminations.

6.1.6. Fine carbonaceous matrix and coatings

Fine carbonaceous material occurs as a trace component within the matrix of some samples (e.g. Fig. 8a). Some grains (particularly in intraclast breccias) have thin coatings (10-50 μm thick) of fine carbonaceous material around the grain edges (Fig. 10a, Supp. Fig. S14). These coatings tend to smooth topography on grain edges, filling indents in surfaces with slightly thicker layers, regardless of grain orientation. Coatings are most common on volcanic grains, but also occur on silica granules and larger silica intraclasts.

6.2. Volcanic material

Sand-sized phenocrysts or other monocrystalline mineral grains are essentially non-existent in upper Mendon rocks, with the exception of a few rare quartz grains. Much more common, however, are sand-sized, angular to subangular sericitic chert grains and other aggregates of microquartz and phyllosilicates (sericite and/or chlorite) (Fig. 10a-c). Some also contain diffuse carbonaceous matter and/or fine iron oxide inclusions. These types of grains occur as a minor component in some laminated black chert and are a common and abundant component of intraclast breccia beds. Accretionary lapilli or aggregates of lapilli (Fig. 10c) are rare and occur mainly in a few intraclast breccias and in graded beds in section SAF 620 (Supp. Fig. S7). The accretionary lapilli contain blocky, non-vesicular pyroclasts and

are similar to those described in ultramafic pyroclastic rocks of the Onverwacht Group (Thompson Stiegler et al., 2008; Thompson Stiegler et al., 2010).

6.3. Silica granules and chert bands

Silica granules, sand-sized sub-spherical silica grains (Stefurak et al., 2014; Stefurak et al., 2015), commonly occur in upper Mendon rocks. Granules are commonly a minor component within black chert dominantly composed of simple and composite carbonaceous grains and intraclast breccia layers containing a variety of grain types. Some white bands within BBWC and BFC can be determined petrographically to be composed entirely of silica granules (Supp. Fig. S15). Silica granules are typically moderately to heavily compacted and display grain-supported and matrix-supported textures in different occurrences. Granule layers are not graded and only rarely display current structures. Aggregates of a few silica granules, granule layer intraclasts, and internally unstructured white chert band fragments are common components of intraclast breccia deposits (Fig. 10d).

6.4. Ferruginous material

Iron typically occurs within fine-grained, finely-laminated chert as <50 µm mineral grains intergrown with microquartz. The most common iron-bearing mineral phases are siderite and goethite, with rare pyrite. Many iron-bearing grains are euhedral. Ferruginous material can be associated with fine carbonaceous material present within the microquartz matrix, rare silica granules, and fine *in situ* carbonaceous laminations (Fig. 10e-f).

6.5. Impact spherules

Previous authors have identified several distinctive beds of impact spherules within the Onverwacht and Fig Tree Groups in the BGB (Lowe and Byerly, 1986; Kyte et al., 2003; Lowe et al., 2003). These spherule beds are not a focus of this study, but rare impact spherules are observed in some intraclast breccias of the upper Mendon Formation. These spherules are texturally similar to those described previously (Lowe and Byerly, 1986; Lowe et al., 2003). Spherules have nearly circular cross

sections and are typically composed of microcrystalline quartz and phyllosilicates (cf. type 3 spherules in Lowe and Byerly, 1986).

6.6. Intraclast breccia point count data

Intraclast breccias are the principal upper Mendon lithofacies that reflect current transport, implying that their compositions could include grains transported from adjacent environments that may not be recorded in the rock record. Furthermore, we can subdivide intraclast breccias into two types based on sedimentological observations – type 1 breccias that reflect local disruption by currents and type 2 breccias that reflect more sustained and widespread current transport and reworking. Outcrops do not always allow the straightforward differentiation of these two subtypes due to limited lateral continuity and the challenges of identifying grain compositions in the field. Point counts provide an independent method to evaluate the hypothesis that intraclast breccias can be subdivided into local and non-local event types and provide additional insights into any associations of grain types.

The most distinctive grain types in intraclast breccia samples are intraclasts that represent different original sedimentary compositions: laminated carbonaceous intraclasts, black chert intraclasts, silica granule aggregates, and chert plates. When the point count data are plotted using poles of simple/composite carbonaceous grains (C); silica granules, silica granule intraclasts, and chert plates (S); and carbonaceous intraclasts and volcanic grains (BLV) (Fig. 11a), no samples have >50% simple/composite carbonaceous grains, a field in which the vast majority of black chert compositions would lie. This is not a surprising result as intraclast breccias, by definition, include a considerable component of coarse intraclasts and would not be expected to be dominated by the finer-grained organic grains. Furthermore, as intraclast breccias are interpreted as storm deposits associated with greater current energy than the background depositional processes, one would expect much of the fine-grained and perhaps low density carbonaceous sediment to have been winnowed out.

The samples can be further divided into those dominated by silica granules and associated intraclasts (S>BLV) versus volcanic material and carbonaceous intraclasts (BLV>S). Focusing on just the different intraclast types (Fig. 11b), the same samples dominated by silica clasts from Fig. 11a are confined to the S corner, defined by >60% chert bands and silica granules. These samples correspond to the Type 1 intraclast breccias lithofacies classification. The remaining samples are dominated by either black chert intraclasts (B) or laminated carbonaceous intraclasts (L), which correspond to the Type 2 intraclast breccias lithofacies classification. If volcanic grains (V) are plotted as the third pole instead of chert bands and granules and we remove the samples dominated by silica clasts (S>60%), the samples fall into two domains (Fig. 11c): those with a greater proportion of black chert intraclasts than laminated carbonaceous intraclasts (B>L, Type B) and those with a greater proportion of laminated carbonaceous intraclasts than black chert intraclasts (L>B, Type L). In fact, the area that would represent similar abundances of both types of distinctive carbonaceous intraclasts is unoccupied by the samples analyzed here.

The amount of matrix and/or cement can also be roughly calculated and compared using the point count analyses (Supp. Table S4). With the exception of a few locally-derived breccias, carbonaceous matrix was less abundant than microquartz matrix and cement (mean ratio of 0.7), suggesting that the original breccia had a high proportion of open pore space between clasts, consistent with the energetic deposition of many intraclast breccias. The percentage of sample area of matrix and cement material ranged from 23% to 64%, with a mean value of 38%, consistent with petrographic observations that most intraclast breccias are loosely packed and uncompacted.

7. Geochemistry

Major element geochemistry confirms field and petrographic observations that Upper Mendon chert lithofacies are dominantly composed of microquartz – all the samples presented here,

representing all the upper Mendon lithofacies, have >90 wt% SiO_2 (Tables 1-3). Iron and aluminum are typically the next most abundant elements, with maximum FeO* (total iron) contents of 6.36 wt% and maximum Al_2O_3 contents of 3.02 wt%. Black chert, included banded black-and-white, massive, and laminated lithofacies, contain less iron and aluminum than other lithofacies that were interpreted based on field and petrographic evidence to contain more ferruginous and/or tuffaceous material: all black chert samples have >97 wt% SiO_2 and <2.5 wt% combined FeO* and Al_2O_3 (Fig. 12). Upper Mendon samples are characterized by low abundances of most trace elements, with the exception of elevated Ba concentrations in samples from the Barite Syncline area (Table 4). Black chert samples have lower overall abundances of REE than lithofacies identified as being more ferruginous or tuffaceous (Fig. 13, Supp. Table S6), consistent with the conclusion that black chert is dominantly composed of silica and carbonaceous material with very low abundances of other trace phases.

8. Discussion

8.1 Sediment sources

Petrographic analyses distinguish four main types of primary sedimentary material present in the upper Mendon Formation: carbonaceous sediments, volcaniclastic sediments, siliceous sediments (i.e. silica granules, granule intraclasts, and white chert plates), and ferruginous sediments. The following discussion will consider the sources of these different types of sediment and their significance for understanding the depositional processes and environments of the upper Mendon Formation.

8.1.1. Carbonaceous sediment

Although SiO_2 in the form of microquartz is the dominant component by weight in the upper Mendon chert analyzed in this study, most of this silica was added during diagenesis and metasomatism (see section 8.3). Based on petrographic observations and point count data, we therefore interpret that carbonaceous grains were the dominant primary sedimentary material in the upper Mendon Formation.

Simple carbonaceous grains (Fig. 8a) are the most common and abundant grain type, but their lack of complex internal structure makes it difficult to uniquely identify how or where these grains originated – whether they originated in the water column or as ripped-up microbial mats. These grains are the dominant primary sedimentary component in fine-grained and finely laminated facies interpreted to represent hemipelagic settling out of the marine water column, so they were certainly relatively abundant and ubiquitous in the water column. Even in the modern ocean, a considerable amount of particulate organic matter cannot yet be definitively connected to a particular composition or origin (Lee et al., 2004). Composite carbonaceous grains present a similar conundrum: were they larger and more complex rip-up clasts of shallower water organic-rich oozes or did they form via the aggregation of simple carbonaceous grains during settling? Whereas small composite grains occur in apparently low energy hemipelagic deposits with simple carbonaceous grains, large and complex composite grains are common in relatively energetic deposits such as intraclast breccia layers likely representing erosion and transport by storms. Carbonaceous material in the matrix is finely disseminated, with no distinguishable grains. This material probably originated as an organic-rich siliceous mud composed of extremely fine organic matter and colloidal silica settling out of the water column.

In situ organic-rich laminations are rare in the upper Mendon Formation. Previous authors have interpreted fine carbonaceous laminations separated by thin chert layers as microbial mats based on the common co-occurrence of roll-up structures, which is interpreted to imply a certain degree of cohesive strength provided by a microbial biofilm or mat (Walsh and Lowe, 1999; Tice and Lowe, 2006). Comparable roll-up structures occur only rarely in upper Mendon Formation samples (Fig. 8g), although this could also be a function of the relative paucity of in situ laminations and the infrequency of currents strong enough to rip up and re-deposit carbonaceous laminations. Of the *in situ* laminations observed, the isolated example in Fig. 9 provides the most convincing evidence for microbial mats. The smooth draping of the laminations over a comparatively large scale of topography (>2 mm relief), the

occurrence on steep surfaces (including an overhanging surface), the apparent "trapping-and-binding" of loose sediment, and the persistence of laminations even when sand-sized detrital grains were still being transported and deposited by currents are all consistent with a biological origin.

In comparison with this example, other types of laminations observed are not unambiguously biogenic (Supp. Fig. S13). For example, these morphologies could possibly represent alternating deposition of organic ooze and extremely fine-grained silica (e.g. colloidal silica, with grain diameters <10 μm) – in other words, a smaller scale and finer-grained version of BBWC. Silica polymerization during earliest diagenesis could have provided a degree of cohesiveness to these laminations, as is observed in the early deformation of some white chert bands (Supp. Fig. S16). These fine laminations typically occur within finely laminated, fine-grained ferruginous lithofacies, indicating that they formed in low-energy settings characterized by relatively slow depositional rates, which could be consistent with either microbial or abiotic mechanisms.

Laminated carbonaceous coatings are also enigmatic. Although the coatings occur on some silica grains, they are most common and best-developed on volcanic grains. Previous studies have identified anaerobic nitrate-dependent Fe(II)-oxidizing organisms capable of utilizing Fe(II) in mineral phases, including goethite, siderite, pyrite, neosilicates, and phyllosilicates (Chaudhuri et al., 2001; Weber et al., 2001; Shelobolina et al., 2003), although other studies have highlighted that Fe(II) oxidation can also occur abiotically by reacting with nitrite, a metabolic intermediate of denitrification (Cooper et al., 2003; Coby and Picardal, 2005; Pantke et al., 2011; Carlson et al., 2012; Picardal, 2012; Kopf et al., 2013). Although it is possible that analogous Fe-oxidizing microbes colonized volcanic grains, one would expect these organisms to have moved inwards as Fe(II) was progressively depleted on the grain edges, implying that the laminations would also have grown inwards rather than outwards. Since the carbonaceous coatings are also observed on some silica granules and intraclasts, it is also possible that these relatively grains simply provided more favorable surfaces for biofilm colonization and that the

apparent selectivity is not strictly related to grain composition or microbial metabolism. Other possibilities are that microbes could have been utilizing Fe(II) and/or other metal cations from these volcaniclastic grains as cofactors for their metabolism rather than as electron donors or that organic molecules collected passively on these grain surfaces without any direct microbial involvement.

Laminated carbonaceous intraclasts (Fig. 8c-e) and black chert intraclasts (Fig. 8f) provide insights into depositional modes of carbonaceous material in shallower water. Their occurrence only within Type 2 intraclast breccias indicates that these clasts originated in a shallower, more energetic environment from which they were periodically ripped up and transported out to deeper waters by storms. Point count data from intraclast breccias suggest that co-occurrence of these two intraclast types is rare – most samples that contain these intraclast types are dominated either by an assemblage of black chert intraclasts and volcanic grains or by laminated carbonaceous intraclasts and volcanic grains (Fig. 11c). This suggests that these two intraclast types originated from different environments, which is consistent with petrographic observations.

Black chert intraclasts are internally composed of mixtures of simple carbonaceous grains, tuffaceous material, and rare silica granules. Black chert matching this description is a common lithofacies in the Mendon Formation and in older cherty units of the Onverwacht Group (Walsh and Lowe, 1999). It is therefore impossible to identify a particular stratigraphic horizon or paleoenvironment from with these intraclasts originated.

The textures observed in laminated carbonaceous intraclasts have not been observed *in situ* within the upper Mendon Formation or in other black cherts in the BGB (Walsh and Lowe, 1999; Tice and Lowe, 2006). The absence of texturally similar laminated carbonaceous matter in chert deposited in shallow water depositional environments such as the basal Buck Reef Chert, characterized by silicified evaporites and wave ripples (Lowe and Fisher Worrell, 1999), and the Msauli Chert (Lowe, 1999c) indicates that the formation of this texture was sensitive to environmental factors – perhaps areas with

less frequent pyroclastic input, compared with the Msauli Chert, or more moderate salinity, compared with the evaporitic member of the Buck Reef Chert.

Laminated carbonaceous intraclasts also provide some of the more convincing evidence of a microbial origin. As with many younger Precambrian stromatolites (Grotzinger and Knoll, 1999), laminations are defined by darker organic-rich layers and lighter, less organic-rich layers, although in the Mendon Formation the mineral composition is microquartz instead of carbonate. It seems likely that in many or all cases, microtopographic relief was produced abiotically through precipitation of cements (Supp. Fig. S11) and/or deposition of detrital material (Fig. 8e). At the same time, the microtextures of laminated carbonaceous intraclasts are dominated by carbonaceous material, rather than by sparry cements. The alternation of dark, organic-rich layers with lighter layers of microquartz cement or silt-sized sediment, combined with steep truncation surfaces (Supp. Fig. S11) and draped laminae (Fig. 8c), both indicating that the laminae were relatively cohesive, are most consistent with the presence of microbial mats rather than a structure created entirely by abiotic mineral precipitation. If these intraclasts indeed represent microbial mats, they likely originated from relatively shallow water within the photic zone – *in situ* laminations observed in the relatively deep waters represented by the upper Mendon are typically thinner and much less organic-rich (Fig. 9, Supp. Fig. S13) than those observed in intraclasts. Other environmental factors like salinity, wave energy, and input of volcanic sand would have made many shallow environments non-ideal for microbial mat growth and likely account for the absence of *in situ* preservation of this texture.

In summary, the present study suggests that the bulk of the organic matter in the upper Mendon Formation was deposited as fine detrital grains that settled as hemipelagic sediment out of the water column. Some of this material was reworked locally by currents. Very little appears to represent *in situ* microbial mats; although inputs of iron or volcanic particles could have provided local geochemical gradients that microbes could exploit, the default situation appears to have been a slow rain of organic

particles with little steady influx of other nutrients or light. Some contrasting larger detrital particles appear to represent microbial mats eroded in shallow water and transported to the local sites of deposition by storms or tsunamis. It is unclear whether all types of organic particles represent material ripped up from microbial mats accumulating in shallow water or whether there might have been Archean planktonic microbes living and dying within the water column.

8.1.2. Volcanic sediment

Inputs of volcanic material are commonly superimposed on the background pattern of sedimentation in the upper Mendon Formation represented by laminated black chert composed of fine carbonaceous grains. Fine volcanic grains occur in some laminated black chert samples, likely representing pulses of ash input from relatively small and/or distant pyroclastic eruptions. Coarser volcanic material, including accretionary lapilli, are most common in intraclast breccias, indicating that high energy storm deposits often transported volcanic detritus in from shallower water environments on volcanic platforms. Previous authors correlated distinct generations of pyroclastic material sedimentologically and geochemically in lower units of the Mendon Formation and from older Onverwacht stratigraphy (Lowe, 1999c; Thompson Stiegler et al., 2010; Thompson Stiegler et al., 2011; Decker et al., 2015). In contrast, although some silicified ashes can be locally traced along strike (Supp. Fig. S1), most cannot. The number and stratigraphic position(s) of pyroclastic layers varies significantly between the various upper Mendon sections, even between those occurring in the same structural belt (Fig. 7) and the ash and accretionary lapilli layers in the upper Mendon Formation are typically quite thin – single laminae or centimeter-scale graded beds. This is consistent with the interpretation that this deposition was far removed from volcanic sites during a period of local volcanic quiescence (Lowe and Byerly, 1999; Thompson Stiegler et al., 2011). Lowe (1994a; 1999a) proposed that upper Mendon time was characterized by active rifting and the relative migration of the volcanic center to the north. This tectonic regime would suggest that the location(s) of volcanism were continually migrating relative to

the various stratigraphic sections, which themselves were also being affected (e.g. changes in depositional water depth due to rifting) and is consistent with the expression of variability of thickness and abundance of volcanic units.

Another factor that likely contributed to the apparent variability in number and stratigraphic positions of silicified ash beds is the difficulties presented by identifying them in outcrop. Many ashes are pervasively silicified and can commonly have >90 wt% SiO_2 (Lowe, 1999b). Although some are easily distinguished by their greenish color, others are whitish to grey or even black when ash is mixed with detrital carbonaceous matter (Lowe, 1999b). Lithological identification based mainly on field observations therefore probably underestimate the number of ash beds, particularly due to the discontinuous nature of outcrops, the higher weathering susceptibility of more tuffaceous and/or ferruginous facies compared to better silicified black chert, and the wide mixing of ash with carbonaceous matter.

8.1.3. Siliceous sediment

Stefurak et al. (2015) concluded that silica granules observed in the Onverwacht and Fig Tree Groups formed via rapid polymerization and aggregation of silica occurring periodically in the shallow water column. The preservation of sedimentary layers composed exclusively of silica granules must have required a relatively slow background depositional rate with little to no input of volcanic grains and a quiet environment below storm wave base, such that other grains were generally not swept in while granules were being deposited and granule layers were generally not reworked by currents. Observed occurrences of silica granules in a wide range of depositional environments, from shallow subtidal to basinal settings, suggest that granules could settle and/or be transported into much deeper water (Stefurak et al., 2014; Stefurak et al., 2015). White chert bands (i.e. primary silica granule layers) tend to be thicker in BBWC than in BFC, the deeper water, more ferruginous lithofacies equivalent, which may reflect a decreased supply of silica granules in deeper waters. Silica granules also commonly occur as a

minor sedimentary component in laminated carbonaceous or ferruginous cherts, indicating that the conditions required to deposit and preserve silica granule layers were not always met. Absence of banded cherts in a particular stratigraphic section could therefore result from a variety of mechanisms - decreases in the production, deposition, and/or preservation of silica granule and granule layers.

The formation of primary silica granules also indicates that the concentration of dissolved silica in seawater was high, at or above saturation with respect to amorphous silica (Stefurak et al., 2014; Stefurak et al., 2015), which is consistent with previous hypotheses (Siever, 1992; Maliva et al., 2005). At these concentrations, silica would mainly occur in colloidal rather than monomeric form (Iler, 1979). In addition to forming sand-sized silica granules (Stefurak et al., 2015), this colloidal silica could also have been deposited as a siliceous mud, mixed with fine particulate organic matter and primary iron phases. This mud mixture was probably a common matrix material in many cherts, particularly those that now contain microquartz matrix with trace inclusions of carbonaceous material and/or iron phases. Finally, the widespread silicification observed in a variety of volcanic and sedimentary lithofacies in the Barberton Greenstone Belt (Lowe, 1999b) indicates that silica was highly mobile during diagenesis and that considerable amounts of silica were added post-depositionally.

8.2.4. Ferruginous material

We interpret that ferruginous lithofacies – laminated grey chert, laminated ferruginous chert, and BFC – represent the deepest water deposits in the Mendon Formation based on sedimentary structures, including the ubiquity of fine-grained sediment and fine laminations and a paucity of intraclast breccias. Iron occurs in the form of siderite, iron oxides (goethite and perhaps hematite), and rare cases of pyrite, all intergrown with microquartz (Fig. 10e-f). Based on cross-cutting relationships and euhedral crystal forms, much of the iron was altered in form and probably composition during diagenesis. The iron probably originally accumulated as hemipelagic rain of mud- to silt-sized iron

particles as ferric or mixed valence oxyhydroxides or clays (Rasmussen et al., 2014; Rasmussen et al., 2015b) and perhaps as siderite (Sawicki et al., 1995; Tice and Lowe, 2004).

The occurrence of iron mainly within deeper water lithofacies suggests that iron deposition was restricted to the deep water column, which is consistent with the hypothesis that the ocean was chemically stratified (Klein and Beukes, 1989; Lowe, 1994b; Tice and Lowe, 2004). Dissolved Fe(II) most likely originated from hydrothermal vents and through low temperature alteration of mafic and ultramafic crust (Jacobsen and Pimentel-Klose, 1988; Bau and Möller, 1993; Hamade et al., 2003). There are a number of abiotic and biologically-mediated mechanisms through which hydrated Fe(III) or mixed valence oxyhydroxides (e.g. "green rust", Zegeye et al., 2012) could have formed, most of which involve oxidation of Fe(II) in the water column by free oxygen or through microbial metabolic activity (Posth et al., 2014). Rasmussen et al. (2014, 2015a, 2015b) suggested that deposition of Fe(II)-rich precursors to iron-bearing clays like ferrosaponite was a significant mode of reduced iron deposition in Archean environments. Indeed, many of the ferruginous samples analyzed in this study contain more iron and aluminum than black cherts (Fig. 12).

There are several pathways through which siderite could have formed. Tice and Lowe (2004) suggested that siderite precipitated at the interface of iron-rich deep waters and shallow CO_2-dominated surface water. Sawicki et al. (1995) demonstrated microbially-mediated precipitation of siderite in a biofilm, which suggests that siderite could have precipitated in situ. Siderite could also have formed through reactions of Fe(II) or Fe(III) oxyhydroxides with organic matter during diagenesis (Köhler et al., 2013; Posth et al., 2013; Posth et al., 2014). The combined effects of diagenesis, metamorphism, and surface oxidation make it difficult to isolate any one primary composition and the original iron-bearing phases probably included a range of mineralogical compositions. The key observation here is the general segregation of iron to deeper water lithofacies, indicating some degree of chemical stratification with respect to iron.

8.2 Marine vs. hydrothermal geochemical signatures

The style of deposition indicated by the sedimentology of the upper Mendon Formation is consistent with a normal relatively deep-water marine setting, where much of the sedimentary material was delivered via slow settling from the overlying water column. However, the question of the degree of hydrothermal influence on this type of chemical sedimentary rock that is uniquely abundant in Precambrian sequences (non-biogenic chert) is difficult to answer with sedimentology alone. Field observations are not consistent with these rocks having formed as direct hydrothermal exhalites. REE geochemistry provides a complementary approach to evaluate the degree of hydrothermal influence, if any, on the compositions of upper Mendon chert. Modern seawater is characterized by several key features in shale-normalized REE data (cf. Bolhar et al., 2004): positive La anomalies, negative Ce anomalies, positive Gd anomalies, elevated Y/Ho above the chondritic value (~26), and depletion of LREE and MREE relative to HREE (La_{SN}/Yb_{SN} <1; Gd_{SN}/Yb_{SN} < 1, where "SN" stands for shale-normalized). The majority of samples analyzed here are consistent with these criteria (Table 5), with the exception of negative Ce anomalies, but this is expected for an anoxic early Archean ocean. The negative Ce anomalies that are observed in these samples probably resulted from post-depositional alteration rather than reflecting ambient Archean seawater redox conditions (Hayashi et al., 2004). Previous authors have applied same set of criteria – positive Y, Gd, and La anomalies and LREE depletion – to conclude that Archean and early Paleoproterozoic cherts formed as marine chemical sediments, including, carbonates and chert from the 3.45 Ga Strelley Pool Chert (Pilbara Craton, Western Australia) (Allwood et al., 2010) and BIF-associated chert from the 2.75-2.7 Ga Abitibi greenstone belt (Thurston et al., 2012) and the ~2.7 Ga Woodburn Lake greenstone belt (Gourcerol et al., 2015), both in Canada.

We observe both weakly positive and weakly negative Eu anomalies (chondrite-normalized). Positive Eu anomalies are typically interpreted to reflect hydrothermal input (Sugitani, 1992) because

modern high temperature hydrothermal fluids have strong positive Eu anomalies (Bau, 1991; Douville et al., 1999). However, weak positive Eu anomalies, including the range observed here, are consistent with Archean seawater due to a stronger hydrothermal influence on seawater chemistry on the early Earth (Allwood et al., 2010). The Eu anomalies presented here are therefore also consistent with a marine origin.

Ferruginous lithofacies (laminated ferruginous chert and BFC) are more enriched in HREE relative to BBWC, while laminated grey chert is more enriched in LREE compared with other lithofacies (Fig. 13b). Contamination from terrestrial input can cause relative enrichment in LREE (e.g. Goldstein and Jacobsen, 1988), which likely explains the signal observed in laminated grey chert, which have higher Al contents than other lithofacies (Fig. 12a), where Al concentration can be used as a proxy for terrigenous input. Severmann et al. (2004) observed HREE enrichment in modern Fe-bearing hydrothermal clays, consistent with the inferred primary mineralogy of fine ferruginous sediment (cf. Rasmussen et al., 2015b).

8.3 Diagenesis and metamorphism

The upper Mendon chert samples analyzed here are currently composed of >90 wt% SiO_2 (Fig. 12, Tables 1-3). Although some silica is primary (e.g. silica granules), much was probably added during diagenetic silicification of primary sediments, whose original compositions as mixtures of carbonaceous, tuffaceous, and ferruginous materials are now reflected as trace concentrations of carbon, alumina, and iron within the chert. Patterns of compaction and post-depositional deformation indicate that the timing of silicification varied between and among particular grain types and lithofacies. Even though silica granules are commonly compacted (Supp. Fig. S15), white chert bands composed of silica granules are also commonly locally brecciated as apparently rigid chert plates (e.g. Fig. 5). These observations indicate that silica granules were originally soft and easily compactible, particularly so because they

were also typically rapidly cemented. In contrast, sand-sized carbonaceous grains in the black chert layers adjacent to white chert bands tend to be equant and apparently uncompacted (e.g. Fig. 8b), even though the early brecciation of white chert bands indicates that the adjacent carbonaceous sediment was silicified later. Many sand-sized grains of organic matter may therefore have been cemented prior to or during deposition, even though the cementation of the pore spaces between these grains apparently occurred much later than in layers of silica granules. At the same time, other black chert samples are composed almost exclusively of compacted simple carbonaceous grains, indicating that not all organic grains were cemented prior to sedimentation. Deeper water lithofacies like laminated grey chert and laminated ferruginous chert generally lack sand-sized sedimentary grains, making it difficult to directly compare the timing of silicification in these environments. Nevertheless, the patterns of relatively early silicification observed in other lithofacies suggest that influx of silica-rich pore fluids occurred early in the diagenetic history of many sediment types, with local variations in timing perhaps resulting from differences in sediment composition affecting the kinetics of silica precipitation.

Beyond the pervasive diagenetic silicification, other aspects of upper Mendon sediments have also been affected by post-depositional changes. Iron occurs within samples in both reduced (siderite and pyrite) and oxidized (goethite and hydrous iron oxides) forms, but cross-cutting relationships of these current mineral phases indicate that they formed during diagenesis and/or metamorphism – sand-sized detrital pyrite, siderite, or hematite grains are not observed. Recent surface oxidation has pervasively affected the redox state and mineralogy of iron in many samples. For example, although siderite is absent from many surface samples of BFC, it is the dominant iron-bearing mineral in this lithofacies within core (Tice and Lowe, 2004). Although siderite could have been primary (Sawicki et al., 1995; Tice and Lowe, 2004), it could also have formed through diagenetic reactions of iron oxyhydroxides and organic matter (Köhler et al., 2013; Posth et al., 2013; Posth et al., 2014). Similarly,

euhedral diagenetic pyrite probably formed during diagenesis via reactions of Fe(II) and sulfide (Taylor and Macquaker, 2000).

The Barberton Greenstone Belt has undergone greenschist-grade metamorphism, experiencing temperatures of ~300°C (Xie et al., 1997; Tice et al., 2004). This has affected the chemical compositions of organic matter and volcaniclastic material within the Mendon Formation. As determined by Raman spectroscopy, organic carbon in the samples occurs as partially disordered carbonaceous matter (Supp. Fig. S9). Although it has not been fully converted to graphite, primary organic material has been degraded and condensed to its current form. Similarly, the grains we interpret as volcaniclastic sand occur as fine-grained aggregates microquartz, chlorite, and sericite, which formed via metasomatism and metamorphism of primary glass and mafic minerals. These patterns of post-depositional changes in chemical composition are consistent with trends observed throughout the Barberton Greenstone Belt (Duchac and Hanor, 1987; Byerly, 1999; Lowe, 1999b; Thompson Stiegler et al., 2008).

8.4 Depositional processes and environments

Upper Mendon sedimentation was characterized by settling of particulate organic matter and, in the deeper settings, fine iron particles from the overlying water column under quiet-water conditions below typical storm wave base (Fig. 14). This was punctuated by occasional influxes of volcanic ash and dust as fine pyroclastic fall deposits, silica granule deposition, and reworking, erosion, and/or deposition by storms or possibly tsunamis. There is a considerable degree of spatial variability in the patterns of these event deposits. In the case of silica granule layers, we interpret that this reflects variations in local conditions influencing silica granule formation (e.g. pH, salinity, and concentration of dissolved silica) in addition to current energy (e.g. post-depositional reworking of granules) and diagenetic conditions. The occurrences of intraclast breccias would likely have been affected by local seafloor topography (e.g. Mendon-age sub-basins suggested by Byerly et al., 1996 and Decker et al., 2015). Petrographic and

geochemical analyses of komatiitic flows and ashes of the Mendon Formation also identified significant local- and regional-scale variability, both in composition and in the sequence of volcanic deposits recorded in different areas (Byerly, 1999; Thompson Stiegler et al., 2010; Decker et al., 2015).

Despite this spatial variability, we can also identify general temporal trends (Fig. 15). With the exception of BH-03, sections from the southernmost structural belt along the Msauli River directly overlie the Msauli Chert (M1c). These sections are characterized by a basal ~10 m unit of which approximately 50% of the thickness is BBWC or BFC with many chert plate breccias (Fig. 6). Some of these breccias were likely produced by local disruption and re-sedimentation of chert bands (intraclast breccia lithofacies Type 1), particularly given the abundance of banded chert, but many have point count compositional assemblages dominated by laminated carbonaceous intraclasts (compositional Type L), indicating they were associated with a greater degree of erosion and transportation (intraclast breccia lithofacies Type 2) (Fig. 11b-c). Two sections (SAF 187 and SAF 191) also contain a distinctive marker unit of M2c, a layer of very coarse accretionary lapilli (Supp. Figs. S2 and S3). The Mendon-Fig Tree contact is not well-exposed in these sections, but the more complete sections (SAF 186 and SAF 187) have uppermost units characterized by laminated ferruginous chert and generally lacking in banded chert. The basal unit of the southern domain sections appears to represent one of the shallowest environments observed in the upper Mendon Formation based on the occurrence of many intraclast breccias and the erosional contact between the Msauli Chert and overlying black chert, commonly including a basal conglomerate. This unit also indicates a prolonged period of local conditions that were favorable for silica granule deposition (notably, section BHR-01, Fig. 7, also includes several meters of BBWC immediately overlying the Msauli Chert). These conditions apparently ceased during the deposition of the upper units, where we interpret that increased abundance of finely laminated ferruginous chert and decreased evidence of storm reworking reflects deepening conditions.

The sections from the northeastern structural belts are more dissimilar from one another (Fig. 7), reflecting in part that they overlie different Mendon volcanic cycles and lie within different structural belts (Fig. 15, Supp. Table S1). Nevertheless, the northeastern sections share general stacking patterns consisting of: 1) a thick lower unit of ferruginous lithofacies, 2) a 5-10 m thick unit dominantly composed of laminated black chert, and 3) a capping 5-10 m thick unit of whitish- to light-grey-weathering fine-grained silicified ash (Fig. 15). The basal unit is dominated by laminated slightly ferruginous grey chert and/or BFC and is observed in all sections but BHR-01. In the middle unit, laminated black chert is interbedded with BBWC, intraclast breccias, and centimeter-scale graded ashy-to-carbonaceous beds. The uppermost unit is only observed in sections BS-03, BS-02, and SAF 620. The tops of most sections can be correlated reasonably well via the apparently conformable contact with the basal Fig Tree Group, which is marked in some cases by spherule bed S2 (sections SAF 521, SAF 620, and CQ-01) or by distinct beds of bladed barite and barite sands (sections BS-02, CQ-01). The transition from ferruginous lithofacies to black chert, intraclast breccias, and pyroclastic fall deposits suggests a relative shoaling and increased volcanic activity.

The hypothesized deepening of M2c sections in the southernmost structural belt is consistent with the interpretation that active rifting was occurring during Mendon time (Lowe, 1994a; Lowe, 1999a), resulting in the transition from a relatively shallow water setting represented by the Msauli Chert (Lowe, 1999c), to moderate depths represented by black chert and banded chert, to relatively deep water represented by finely laminated ferruginous chert (Fig. 16a-b). Deep water deposition is also recorded in the basal sections of M3c2, M4c, and M5c (Fig. 16c-e). However, these sections also record a series of coherent lithologic changes upsection that reflect gradual shoaling, as represented by the transition from ferruginous lithofacies to black chert, intraclast breccias, and pyroclastic fall deposits (Fig. 7). The observation of this shoaling-upwards trend in sections from different structural belts and overlying different Mendon volcanic cycles suggest that much of this deposition occurred after rifting-

related extension had ceased locally (Fig. 16f). While the M2c sections in the southernmost structural belt record the initial deepening that is not captured by M3c2, M4c, and M5c sections in the eastern domain, they also likely represent condensed sections of post-M3v time, including post-M5v shoaling.

As discussed in section 2, the 50-70 m of upper Mendon Formation stratigraphy could represent up to ~75 Myr. Aside from the erosional contact between the Msauli Chert and the overlying black chert in the southern domain sections, we observe no evidence for extended subaerial exposure or hiatuses in deposition. Sedimentological observations presented here indicate that the upper Mendon Formation was dominantly deposited via slow suspension sedimentation in quiet-water settings (Fig. 14). We therefore conclude that the upper Mendon Formation likely represents nearly continuous, if very slow, sedimentation, with average rates on the order of 0.5-1 mm/kyr. Tice and Lowe (2006) also interpreted slow depositional rates for the Buck Reef Chert, a thick chert unit in the Kromberg Formation, an older part of the Onverwacht Group. Thurston et al. (2008) inferred similarly slow depositional rates for sedimentary units separating volcanic episodes in the ~2.7 Ga Abitibi Greenstone Belt and drew comparisons with the very slow sedimentation in the modern central Pacific Ocean, a depositional setting with essentially no terrigenous input (Gleason et al., 2004). Sedimentation rate likely varied laterally, temporally, and with paleo water depth, depending on the fluxes of the main sediment sources. The lithofacies described here are common in older parts of the Onverwacht Group and other Archean greenstone belts; we can therefore infer that very slow depositional rates and limited terrigenous input were typical in these settings.

9. Conclusions

The upper Mendon Formation is characterized by ~20-70 m of mainly fine-grained sediments now represented by a variety of cherts. The dominant lithofacies are black chert and slightly ferruginous grey chert. Banded black-and-white and/or ferruginous chert, silicified ashes, and intraclast breccia units

are subordinate lithofacies in terms of total thickness, but are significant in that they record the superimposition of silica granule generation, volcanic episodes, and storm or tsunami events, respectively, on the background deposition represented by the black and grey chert. This background deposition occurred via slow settling of simple and composite carbonaceous grains and, in the deepest areas, iron-bearing materials into low energy depositional environments below and in some cases well below storm wave base. This environment would not have been ideal for the development of thick microbial mats – it was almost certainly below the photic zone and the supply of nutrients (both P and metals) was probably low due to the low energy setting and relative rarity of inputs of minerals in the form of volcanic materials. This is consistent with the dominance of particulate carbonaceous material over *in situ* carbonaceous laminations. The morphologies of simple and composite carbonaceous grains cannot be unambiguously tied to a biogenic origin, but some *in situ* laminations, many laminated carbonaceous intraclasts, and laminated carbonaceous coatings on volcanic grains provide more convincing textural and morphological evidence for life in the form of microbial mats or biofilms. Pyroclastic fall deposits occur mainly as thin layers, consistent with the previous interpretation that uppermost Mendon time represented a period of local volcanic quiescence (Lowe and Byerly, 1999). Although some silicified ashes can be traced between sections, the abundance and stratigraphic locations of volcaniclastic units shows significant variation. Previous observations of the petrography and geochemistry of Mendon komatiites and ashes also suggest significant lateral variability, likely reflecting the wide areal extent of original Mendon deposition and local topographic effects. Lithofacies patterns in both sets of sections are consistent with the interpretation that Mendon time was characterized by rifting (Lowe, 1994a; Lowe, 1999a), recorded as deepening in the older, lowest cycle upper Mendon sections in the southern domain and the relatively deep water ferruginous bases of the higher cycle sections in the northeastern domain, and then gradual shoaling, likely after rifting-related

extension had ceased, before the emplacement of impact layer S2 marking the boundary with the overlying Fig Tree Group.

Acknowledgments

We thank the following for their help in the field: G. Byerly, D. Zentner, K. McManus, N. Decker, M. Malkowski, and N. Drabon. E. J. T. was supported by an NSF Graduate Fellowship and McGee and Shell Grants from the School of Earth Sciences, Stanford University. This study was carried out using funds provided by the School of Earth Sciences, Stanford University, to D. R. L. The authors are grateful to Sappi Forest Products, the Mpumalanga Parks Board (J. Eksteen and L. Loocks), and Taurus Estates (C. Wille) for access to private properties. We thank Editor R. Parrish, A. Hofmann, P. Thurston, and an anonymous reviewer for their helpful comments, which have substantially improved the manuscript.

References

Allwood, A.C., Kamber, B.S., Walter, M.R., Burch, I.W., Kanik, I., 2010. Trace elements record depositional history of an Early Archean stromatolitic carbonate platform. Chemical Geology 270 (1), 148-163.

Armstrong, R.A., Compston, W., de Wit, M.J., Williams, I.S., 1990. The stratigraphy of the 3.5-3.2 Ga Barberton Greenstone Belt revisited: a single zircon ion microprobe study. Earth and Planetary Science Letters 101 (90-106).

Bau, M., 1991. Rare-earth element mobility during hydrothermal and metamorphic fluid-rock interaction and the significance of the oxidation state of europium. Chemical Geology 93 (3), 219-230.

Bau, M., Möller, P., 1993. Rare earth element systematics of the chemically precipitated component in early Precambrian iron formations and the evolution of the terrestrial atmosphere-hydrosphere-lithosphere system. Geochimica et Cosmochimica Acta 57 (10), 2239-2249.

Bolhar, R., Kamber, B.S., Moorbath, S., Fedo, C.M., Whitehouse, M.J., 2004. Characterisation of early Archaean chemical sediments by trace element signatures. Earth and Planetary Science Letters 222 (1), 43-60.

Byerly, G.R., 1999. Komatiites of the Mendon Formation: Late-stage ultramafic volcanism in the Barberton Greenstone Belt. In: D.R. Lowe and G.R. Byerly (Editors), Geologic Evolution of the Barberton Greenstone Belt, South Africa. Geological Society of America, Boulder, Colorado, pp. 189-211.

Byerly, G.R., Kroner, A., Lowe, D.R., Todt, W., Walsh, M.M., 1996. Prolonged magmatism and time contraints for sediment deposition in the early Archean Barberton greenstone belt: evidence from the Upper Onverwacht and Fig Tree Groups. Precambrian Research 78, 125-138.

Cantalamessa, G., Di Celma, C., 2005. Sedimentary features of tsunami backwash deposits in a shallow marine Miocene setting, Mejillones Peninsula, northern Chile. Sedimentary Geology 178 (3-4), 259-273.

Carlson, H.K., Clark, I.C., Melnyk, R.A., 2012. Toward a mechanistic understanding of anaerobic nitrate-dependent iron oxidation: balancing electron uptake and detoxification. Frontiers in Microbiology 3 (57), 1-6.

Chaudhuri, S.K., Lack, J.G., Coates, J.D., 2001. Biogenic Magnetite Formation through Anaerobic Biooxidation of Fe(II). Applied and Environmental Microbiology 67 (6), 2844-2848.

Coby, A.J., Picardal, F.W., 2005. Inhibition of NO3− and NO2− Reduction by Microbial Fe(III) Reduction: Evidence of a Reaction between NO2− and Cell Surface-Bound Fe2+. Applied and Environmental Microbiology 71 (9), 5267-5274.

Cooper, D.C., Picardal, F.W., Schimmelmann, A., Coby, A.J., 2003. Chemical and Biological Interactions during Nitrate and Goethite Reduction by Shewanella putrefaciens 200. Applied and Environmental Microbiology 69 (6), 3517-3525.

Dawson, A.G., Stewart, I., 2007. Tsunami deposits in the geological record. Sedimentary Geology 200 (3-4), 166-18.

Decker, N.B., Byerly, G.R., Stiegler, M.T., Lowe, D.R., Stefurak, E., 2015. High resolution tephra and U/Pb chronology of the 3.33–3.26 Ga Mendon Formation, Barberton Greenstone Belt, South Africa. Precambrian Research 261, 54-74.

Douville, E. et al., 1999. Yttrium and rare earth elements in fluids from various deep-sea hydrothermal systems. Geochimica et Cosmochimica Acta 63 (5), 627-643.

Downs, R., 2006. The RRUFF Project: an integrated study of the chemistry, crystallography, Raman and infrared spectroscopy of minerals, The 19th General Meeting of the International Mineralogical Association, Kobe, Japan, pp. O03-13.

Duchac, K.C., Hanor, J.S., 1987. Origin and timing of the metasomatic silicification of an early Archean komatiite sequence, Barberton Mountain Land, South Africa. Precambrian Research 37, 125-146.

Fujino, S., Masuda, F., Tagomori, S., Matsumoto, D., 2006. Structure and depositional processes of a gravelly tsunami deposit in a shallow marine setting: Lower Cretaceous Miyako Group, Japan. Sedimentary Geology 187 (3–4), 127-138.

Gleason, J. et al., 2004. Age calibration of piston core EW9709-07 (equatorial central Pacific) using fish teeth Sr isotope stratigraphy. Palaeogeography, Palaeoclimatology, Palaeoecology 212 (3), 355-366.

Goldstein, S.J., Jacobsen, S.B., 1988. Rare earth elements in river waters. Earth and Planetary Science Letters 89 (1), 35-47.

Gourcerol, B., Thurston, P., Kontak, D., Côté-Mantha, O., 2015. Interpretations and implications of LA ICP-MS analysis of chert for the origin of geochemical signatures in banded iron formations (BIFs) from the Meadowbank gold deposit, Western Churchill Province, Nunavut. Chemical Geology 410, 89-107.

Grotzinger, J.P., Knoll, A.H., 1999. Stromatolites in Precambrian Carbonates: Evolutionary Mileposts or Environmental Dipsticks? Annual Review of Earth and Planetary Sciences 27 (1), 313-358.

Hamade, T., Konhauser, K.O., Raiswell, R., Goldsmith, S., Morris, R.C., 2003. Using Ge/Si ratios to decouple iron and silica fluxes in Precambrian banded iron formations. Geology 31 (1), 35-38.

Hayashi, T., Tanimizu, M., Tanaka, T., 2004. Origin of negative Ce anomalies in Barberton sedimentary rocks, deduced from La–Ce and Sm–Nd isotope systematics. Precambrian Research 135 (4), 345-357.

Iler, R.K., 1979. The Chemistry of Silica. John Wiley & Sons, New York, 866 pp.

Jacobsen, S.B., Pimentel-Klose, M.R., 1988. A Nd isotopic study of the Hamersley and Michipicoten banded iron formations: the source of REE and Fe in Archean oceans. Earth and Planetary Science Letters 87 (1-2), 29-44.

Klein, C., Beukes, N.J., 1989. Geochemistry and sedimentology of a facies transition from limestone to iron-formation deposition in the early Proterozoic Transvaal Supergroup, South Africa. Economic Geology 84 (7), 1733-1774.

Köhler, I., Konhauser, K.O., Papineau, D., Bekker, A., Kappler, A., 2013. Biological carbon precursor to diagenetic siderite with spherical structures in iron formations. Nat Commun 4, 1741.

Kopf, S.H., Henny, C., Newman, D.K., 2013. Ligand-Enhanced Abiotic Iron Oxidation and the Effects of Chemical versus Biological Iron Cycling in Anoxic Environments. Environmental Science & Technology 47 (6), 2602-2611.

Kyte, F.T., Shukolyukov, A., Lugmair, G.W., Lowe, D.R., Byerly, G.R., 2003. Early Archean spherule beds: Chromium isotopes confirm origin through multiple impacts of projectiles of carbonaceous chondrite type. Geology 31 (3), 283-286.

Lahaye, Y. et al., 1995. The influence of alteration on the trace-element and Nd isotopic compositions of komatiites. Chemical Geology 126, 43-64.

Lee, C., Wakeham, S., Arnosti, C., 2004. Particulate Organic Matter in the Sea: The Composition Conundrum. Ambio 33 (8), 565-575.

Lowe, D.R., 1994a. Accretionary history of the Archean Barberton Greenstone Belt (3.55-3.22 Ga), southern Africa. Geology 22, 1099-1102.

Lowe, D.R., 1994b. Early environments: Constraints and opportunities for early evolution. In: S. Bengtson, J. Bergström, G. Vidal and A. Knoll (Editors), Early Life on Earth. Nobel Symposium. Columbia University Press, New York, pp. 24-35.

Lowe, D.R., 1999a. Geologic evolution of the Barberton Greenstone Belt and vicinity. In: D.R. Lowe and G.R. Byerly (Editors), Geologic Evolution of the Barberton Greenstone Belt, South Africa. Geological Society of America, Boulder, Colorado, pp. 287-312.

Lowe, D.R., 1999b. Petrology and sedimentology of cherts and related silicified sedimentary rocks in the Swaziland Supergroup. In: D.R. Lowe and G.R. Byerly (Editors), Geologic Evolution of the Barberton Greenstone Belt, South Africa. Geological Society of America, Boulder, Colorado, pp. 83-114.

Lowe, D.R., 1999c. Shallow-water sedimentation of accretionary lapilli-bearing strata of the Msauli Chert: Evidence of explosive hydromagmatic komatiitic volcanism. In: D.R. Lowe and G.R. Byerly (Editors), Geologic Evolution of the Barberton Greenstone Belt, South Africa. Geological Society of America, Boulder, Colorado, pp. 213-232.

Lowe, D.R., 2013. Crustal fracturing and chert dike formation triggered by large meteorite impacts, ca. 3.260 Ga, Barberton greenstone belt, South Africa. Geological Society of America Bulletin 125 (5-6), 894-912.

Lowe, D.R., Byerly, G.R., 1986. Early Archean silicate spherules of probable impact origin, South Africa and Western Australia. Geology 14 (1), 83-86.

Lowe, D.R., Byerly, G.R., 1999. Stratigraphy of the west-central part of the Barberton Greenstone Belt, South Africa. In: D.R. Lowe and G.R. Byerly (Editors), Geological Evolution of the Barberton Greenstone Belt, South Afric. Geological Society of America, Boulder, Colorado, pp. 1-36.

Lowe, D.R., Byerly, G.R., Heubeck, C., 1999. Structural divisions and development of the west-central part of the Barberton Greenstone Belt. In: D.R. Lowe and G.R. Byerly (Editors), Geological

Evolution of the Barberton Greenstone Belt, South Afric. Geological Society of America, Boulder, Colorado, pp. 37-82.

Lowe, D.R., Byerly, G.R., Heubeck, C., 2012. Geologic Map of the Barberton Greenstone Belt, South Africa. GSA Maps and Charts.

Lowe, D.R. et al., 2003. Spherule beds 3.47-3.24 billion years old in the Barberton Greenstone Belt, South Africa: a record of large meteorite impacts and their influence on early crustal and biological evolution. Astrobiology 3 (1), 7-48.

Lowe, D.R., Fisher Worrell, G., 1999. Sedimentology, mineralogy, and implications of silicified evaporites in the Kromberg Formation, Barberton Greenstone Belt, South Africa. In: D.R. Lowe and G.R. Byerly (Editors), Geologic Evolution of the Barberton Greenstone Belt, South Africa. Geological Society of America, Boulder, Colorado, pp. 167-188.

Lowe, D.R., Nocita, B.W., 1999. Foreland basin sedimentation in the Mapepe Formation, southern-facies Fig Tree Group. In: D.R. Lowe and G.R. Byerly (Editors), Geologic Evolution of the Barberton Greenstone Belt, South Africa. Geological Society of America, Boulder, Colorado, pp. 233-258.

Maliva, R.G., Knoll, A.H., Simonson, B.M., 2005. Secular change in the Precambrian silica cycle: Insights from chert petrology. GSA Bulletin 117 (7/8), 835-845.

Massari, F., D'Alessandro, A., 2000. Tsunami-related scour-and-drape undulations in Middle Pliocene restricted-bay carbonate deposits (Salento, south Italy). Sedimentary Geology 135 (1-4), 265-281.

Pantke, C. et al., 2011. Green Rust Formation during Fe(II) Oxidation by the Nitrate-Reducing Acidovorax sp. Strain BoFeN1. Environmental Science & Technology 46 (3), 1439-1446.

Paris, I., Stanistreet, I.G., Hughes, M.J., 1985. Cherts of the Barberton Greenstone Belt Interpreted as Products of Submarine Exhalative Activity. The Journal of Geology 93 (2), 111-129.

Picardal, F.W., 2012. Abiotic and microbial interactions during anaerobic transformations of Fe(II) and NO_x^-. Frontiers in Microbiology 3 (112), 1-7.

Posth, N.R., Canfield, D.E., Kappler, A., 2014. Biogenic Fe(III) minerals: From formation to diagenesis and preservation in the rock record. Earth-Science Reviews.

Posth, N.R. et al., 2013. Simulating Precambrian banded iron formation diagenesis. Chemical Geology 362 (0), 66-73.

Rasmussen, B., Krape , B., Meier, D.B., 2014. Replacement origin for hematite in 2.5 Ga banded iron formation: Evidence for postdepositional oxidation of iron-bearing minerals. Geological Society of America Bulletin.

Rasmussen, B., Krapež, B., Muhling, J.R., 2015a. Seafloor silicification and hardground development during deposition of 2.5 Ga banded iron formations. Geology 43 (3), 235-238.

Rasmussen, B., Krapež, B., Muhling, J.R., Suvorova, A., 2015b. Precipitation of iron silicate nanoparticles in early Precambrian oceans marks Earth's first iron age. Geology 43 (4), 303-306.

Sawicki, J.A., Brown, D.A., Beveridge, T.J., 1995. Microbial precipitation of siderite and protoferrihydrite in a biofilm. The Canadian Mineralogist 33 (1), 1-6.

Severmann, S., Mills, R.A., Palmer, M.R., Fallick, A.E., 2004. The origin of clay minerals in active and relict hydrothermal deposits. Geochimica et Cosmochimica Acta 68 (1), 73-88.

Shelobolina, E.S., VanPraagh, C.G., Lovley, D.R., 2003. Use of Ferric and Ferrous Iron Containing Minerals for Respiration by Desulfitobacterium frappieri. Geomicrobiology Journal 20 (2), 143.

Siever, R., 1992. The silica cycle in the Precambrian. Geochimica et Cosmochimica Acta 56, 3265-3272.

Stefurak, E.J., Lowe, D.R., Zentner, D., Fischer, W.W., 2015. Sedimentology and geochemistry of Archean silica granules. Geological Society of America Bulletin, B31181. 1.

Stefurak, E.J.T., Lowe, D.R., Zentner, D., Fischer, W.W., 2014. Primary silica granules – A new mode of early Archean sedimentation. Geology 42 (4), 283-286.

Sugitani, K., 1992. Geochemical characteristics of Archean cherts and other sedimentary rocks in the Pilbara Block, Western Australia: evidence for Archean seawater enriched in hydrothermally-derived iron and silica. Precambrian Research 57 (1-2), 21-47.

Taylor, K.G., Macquaker, J.H.S., 2000. Early diagenetic pyrite morphology in a mudstone-dominated succession: the Lower Jurassic Cleveland Ironstone Formation, eastern England. Sedimentary Geology 131 (1–2), 77-86.

Taylor, S.R., McLennan, S.M., 1985. The Continental Crust: Its Composition and Evolution. Blackwell, Oxford, 312 pp.

Thompson Stiegler, M., Lowe, D.R., Byerly, G.R., 2008. Abundant pyroclastic komatiitic volcanism in the 3.5-3.2 Ga Barberton greenstone belt, South Africa. Geology 36 (10), 779-782.

Thompson Stiegler, M., Lowe, D.R., Byerly, G.R., 2010. The petrogenesis of volcaniclastic komatiites in the Barberton Greenstone Belt, South Africa: a textural and geochemical study. Journal of Petrology 51, 947-972.

Thompson Stiegler, M., Lowe, D.R., Byerly, G.R., 2011. Fragmentation and dispersal of komatiitic pyroclasts in the 3.5-3.2 Ga Onverwacht Group, Barberton greenstone belt, South Africa. Geological Society of America Bulletin 123, 1112-1126.

Thurston, P., Ayer, J., Goutier, J., Hamilton, M., 2008. Depositional gaps in Abitibi greenstone belt stratigraphy: a key to exploration for syngenetic mineralization. Economic Geology 103 (6), 1097-1134.

Thurston, P., Kamber, B., Whitehouse, M., 2012. Archean cherts in banded iron formation: insight into Neoarchean ocean chemistry and depositional processes. Precambrian Research 214, 227-257.

Tice, M.M., Bostick, B.C., Lowe, D.R., 2004. Thermal history of the 3.5-3.2 Ga Onverwacht and Fig Tree Groups, Barberton greenstone belt, South Africa, inferred by Raman microspectroscopy of carbonaceous material. Geology 32 (1), 37-40.

Tice, M.M., Lowe, D.R., 2004. Photosynthetic microbial mats in the 3,416-Myr-old ocean. Nature 431, 549-552.

Tice, M.M., Lowe, D.R., 2006. The origin of carbonaceous matter in pre-3.0 Ga greenstone terrains: A review and new evidence from the 3.42 Ga Buck Reef Chert. Earth Science Reviews 76, 259-300.

Walsh, M.M., 1989. Carbonaceous cherts of the Swaziland Supergroup, Barberton Mountain Land, South Africa. Dissertation Thesis, Louisiana State University, Baton Rouge, LA, 119 pp.

Walsh, M.M., Lowe, D.R., 1999. Modes of accumulation of carbonaceous matter in the early Archean: A petrographic and geochemical study of the carbonaceous cherts of the Swaziland Supergroup. In: D.R. Lowe and G.R. Byerly (Editors), Geologic Evolution of the Barberton Greenstone Belt, South Africa. Geological Society of America, Boulder, Colorado, pp. 115-132.

Weber, K.A., Picardal, F.W., Roden, E.E., 2001. Microbially Catalyzed Nitrate-Dependent Oxidation of Biogenic Solid-Phase Fe(II) Compounds. Environmental Science & Technology 35 (8), 1644-1650.

Xie, X., Byerly, G.R., Ferrell, R.E., Jr., 1997. IIb trioctahedral chlorite from the Barberton greenstone belt: Crystal structure and rock composition constraints with implications to geothermometry. Contributions to Mineralogy and Petrology 126, 275-291.

Yui, T.-F., Huang, E., Xu, J., 1996. Raman spectrum of carbonaceous material: a possible metamorphic grade indicator for low-grade metamorphic rocks. Journal of Metamorphic Geology 14, 115-124.

Zegeye, A. et al., 2012. Green rust formation controls nutrient availability in a ferruginous water column. Geology.

Figure Captions

Fig. 1. General stratigraphic column of the volcano-sedimentary sequence in the Barberton Greenstone Belt (left, after Lowe and Byerly, 1999) and overview map of South Africa showing the general location of the Barberton Greenstone Belt (right). Abbreviations: M – Mendon Formation, FTG – Fig Tree Group, and MG – Moodies Group.

Fig. 2. General geologic map of the Barberton Greenstone Belt in the study area, modified after Lowe and Byerly, 1999 and Lowe et al., 2012). Stratigraphic section locations are shown with white stars and character strings (e.g. SAF 186, BH-03) refer to section names. Location map (lower right) shows orientation of map area within general outline of Barberton Greenstone Belt. Some faults and intrusions in the Komati, Hooggenoeg, and Kromberg Formations are not shown. Abbreviations: GGF – Granville Grove Fault.

Fig. 3. Hand sample and field photos of lithofacies of the upper Mendon Formation. (a) Hand sample of a typical faintly laminated black chert. (b) Preserved ripple form and internal cross-laminations in ashy black chert. Ashy layers are light grey; carbonaceous layers are dark grey to black. (c) Centimeter-scale graded beds. Beds grade from dominated by ashy material at the base (lighter grey) to carbonaceous material at the tops (black). (d) Interbedded laminated (lam.) and massive (mass.) grey chert (GC, upper half of image) and banded ferruginous chert (BFC, lower half of image). (e) Banded black-and-white chert (BBWC) showing syndepositional deformation of thin black chert layer (dashed black line). Black (B) and white (W) bands are distinguished. (f) Banded ferruginous chert showing load structure (arrow) of laminated ferruginous chert (F) foundering into underlying white chert band (W). (g) Green cm-scale silicified ash layers (arrows) and overlying cross-bedded ash and white chert composed of silica granules (dashed lines).

Fig. 4. Detailed stratigraphic sections from the Barite Syncline area showing correlation of distinctive intraclast breccia unit and possible correlation of an overlying chert plate breccia composed of thick, flat-lying white chert plates. The BS-03 sections are separated from each other by tens of meters and the BS-02 section is about 500 m away.

Fig. 5. Field photos of distinctive intraclast breccia containing extremely thin chert plates and rounded black chert intraclasts from the Barite Syncline location (see Fig. 4). Exclusive of the chert plates, the breccia layer is weakly graded such that the clasts at the base are, on average, coarser than those nearer the tops. Note that the chert plates appear imbricated, although the direction of imbrication appears to reverse in both beds.

Fig. 6. Simplified stratigraphic sections of the upper Mendon Formation in exposures in the southernmost structural belt along the Msauli River (see Fig. 2), shown from west to east. More detailed versions of sections SAF 186, SAF 187, SAF 625, and SAF 191 are shown in Supp. Figs. S2-S5. Vertical lines at the base of each stratigraphic column represent one meter.

Fig. 7. Simplified stratigraphic sections of the upper Mendon Formation in northeastern structural belts (see Fig. 2), shown from west to east. More detailed versions of sections BS-01, BS-02, BM-01, SAF 620 (upper section), and CQ-01 are shown in Supp. Figs. S1 and S6-S8. Vertical lines at the base of each stratigraphic column represent one meter.

Fig. 8. Photomicrographs of carbonaceous grains and laminations. (a) Simple carbonaceous grains, slightly compacted, within a matrix of microquartz containing finely disseminated carbonaceous material. (b) Composite carbonaceous grains in a relatively uncompacted, grain-supported sandstone.

(c) Flat-laminated carbonaceous intraclasts with a second generation of laminations draped over an edge. The two generations of laminations appear to be cemented together, suggesting that the flat-laminated section was ripped up and locally redeposited, the second generation of laminations draped over and were cemented, and then the whole assemblage was ripped up again and transported into deeper water as a storm or tsunami deposit. (d) Laminated carbonaceous intraclast including overlying layer of sericitic chert interpreted to have originated as fine silicified ash. (e) Large, elongate intraclast with small domal structures overlying cement layers (arrows). (f) Example of non-laminated carbonaceous intraclast, an intraclast type interpreted here as large lithic grains of black chert. In contrast to composite carbonaceous grains, these intraclasts are typically very large (>2 mm), have relatively smooth edges and subangular to rounded shapes, and commonly include silica grains and/or tuffaceous material in addition to carbonaceous material. The matrix to these large clasts contains very fine- to silt-sized simple carbonaceous grains, making the grain boundaries only faintly distinguishable. (g) Rare occurrence of roll-up structure of thin carbonaceous laminations.

Fig. 9. Photomicrograph of thin carbonaceous laminations draped over coarse intraclasts and carbonaceous and volcanic sand grains. Laminations are continuous across complex millimeter-scale topography, exhibiting steep slopes and, in one case, appearing to contour around an overhang. This structure is from an oriented sample and is shown oriented stratigraphically up.

Fig. 10. Photomicrographs of representative volcanic material, silica granules, and ferruginous material. (a) Volcanic sand grains with finely laminated carbonaceous coatings. (b) Blocky, fine-sand-sized pyroclasts and other microquartz-phyllosilicate aggregates. (c) Large intraclast of accretionary lapilli, which themselves contain blocky pyroclasts. (d) Large, irregular intraclast of loosely packed, uncompacted to slightly-compacted silica granules. (e-f) Ferruginous material from laminated grey chert

in plane-polarized transmitted light (e) and reflected light (f), including a few silica granules (upper half of image) and fine *in situ* laminations (lower part of image). Siderite (brightest phase) and goethite (darkest phase) can be distinguished in reflected light (f).

Fig. 11. Ternary diagrams of point count data from intraclast breccia thin sections. Samples are distinguished by stratigraphic section. Abbreviations for poles: C – simple and composite carbonaceous grains, S – silica granules, granule aggregates, and thin white chert plates, B – black chert intraclasts, L – laminated carbonaceous intraclasts, and V – volcanic grains, including microquartz-phyllosilicate aggregates and accretionary lapilli. In (c), the samples dominated by locally-derived intraclasts (S) have been omitted. See Supp. Table S5 for complete point count data set.

Fig. 12. Comparisons of iron and alumina contents of different lithofacies in the upper Mendon Formation. (a) Total iron (FeO*) versus Al_2O_3 (both in wt%). Black chert samples have <2.5 wt% combined iron and alumina, whereas other lithofacies have >2.5 wt% FeO* + Al_2O_3. (b) Combined FeO* + Al_2O_3 versus SiO_2 (both in wt%). As in (a), black chert samples have <2.5 wt% FeO* + Al_2O_3 and >97 wt% SiO_2. Other lithofacies have 90-97 wt% SiO_2. In most samples, the assemblage of SiO_2 + FeO* + Al_2O_3 makes up >98 % of the sample by weight.

Fig. 13. REE diagrams for samples representing major upper Mendon Formation lithofacies. REE abundances are normalized to chondrite (a) and post-Archean Australian average shale (PAAS) (b). An average REE value for Mendon Formation komatiites from Lahaye et al. is also provided for comparison. [1]Chondrite and PAAS values from Taylor and McLennan et al. (1985) [2]Mendon komatiites from Lahaye et al. (1995). See Supp. Table S6 for REE data.

Fig. 14. Schematic illustration of dominant modes of sedimentation recorded in the upper Mendon Formation. Fine particulate carbonaceous and (in deeper waters) ferruginous material are the dominant background sedimentary components, punctuated by periodic inputs of volcanic material and silica granules. Upper Mendon sedimentary rocks were deposited below storm wave base, but include some intraclast breccia deposits with grains that were likely eroded from shallower waters, including densely laminated carbonaceous material.

Fig. 15. Simplified stratigraphic columns showing stratigraphic correlations. Sections in the southern structural belt along the Msauli River contain the Msauli Chert at their base; two of these sections also contain a distinctive marker bed of M2c. Stratigraphic sections in northeastern structural belts overly different volcanic cycles, but can be correlated using the contact with the overlying Mapepe Formation.

Fig. 16. Schematic illustration of the evolution of Mendon Formation volcanic (M1v, M2v, M3v, M4v, and M5v) and sedimentary units (M1c, M2c, M3c, M4c, and M5c). (a) The earliest Mendon volcanic episode (M1v) was emplaced on top of older Onverwacht rocks (Onv, thickness not to scale), which had already been intruded by a suite of TTG plutons (tonalite-trondjhemite-granodiorite), and was subsequently capped by a sedimentary unit (M1c). (b-e) This was followed by four more volcanic episodes, each capped with sedimentary rocks. Sedimentary sections including M1c (e.g. SAF 187, SAF 625, SAF 191) are interpreted to have moved farther from the locus of volcanism (i.e. rift axis) and into deeper water during this time. (f) Upon the cessation of Mendon volcanism, M5c units record a gradual shoaling that is not observed in the condensed sections that are floored with M1c. Suggested relative locations of stratigraphic sections are consistent with the interpretation that the onset of upper Mendon sedimentation was diachronous, with sections overlying M1v representing the oldest and most condensed sections, while sections overlying M5v are the youngest.

Table 1 – Banded black-and-white chert major element geochemistry, weight %, normalized to 100% on a volatile-free basis

Sample	**SAF 23-195**	**SAF 521-3**	**SAF 521-10**	**MW-41-2**	**SAF 199-10**
Source	Lowe 1999	This study	This study	Walsh 1989	This study
Formation	Kromberg	Mendon	Fig Tree	Mendon	Mendon
Lithology	BBWC	BBWC	BBWC	BBWC	BBWC
SiO_2	99.56	99.42	98.68	98.58	98.35
Al_2O_3	0.17	0.21	0.69	0.08	0.49
TiO_2	<d.l.[a]	0.01	0.04	0.01	0.02
FeO*	0.07	0.11	0.14	1.04	0.82
MnO	<d.l.[a]	<d.l.[a]	<d.l.[a]	<d.l.[a]	0.06
CaO	0.03	0.09	0.13	0.22	0.19
MgO	0.12	0.08	0.11	0.02	0.01
K_2O	0.04	<d.l.[a]	0.01	<d.l.[a]	0.01
Na_2O	<d.l.[a]	0.06	0.19	0.03	0.05
P_2O_5	<d.l.[a]	0.01	0.01	0.02	0.01

[a]Concentrations were below detection limit.

Table 2 – Black chert major element geochemistry, weight %, normalized to 100% on a volatile-free basis

Sample	**MW-43-1**	**SAF 115-3**	**SAF 36-57**	**SAF 483-1**	**MW-59-8**
Source	Walsh 1989	Lowe 1999	Lowe 1999	This study	Walsh 1989
Formation	Mendon	Fig Tree	Hooggenoeg	Mendon	Hooggenoeg
Lithology	Massive BC	Massive BC	Massive BC	Lam. BC	Lam. BC
SiO_2	99.02	98.99	99.27	97.57	97.40
Al_2O_3	0.26	0.68	0.48	0.60	0.33
TiO_2	0.01	0.03	0.01	0.02	0.02
FeO*	0.49	0.07	0.04	1.60	2.01
MnO	<d.l.[a]	<d.l.[a]	<d.l.[a]	<d.l.[a]	<d.l.[a]
CaO	0.12	0.09	<d.l.[a]	0.03	0.15
MgO	0.02	<d.l.[a]	0.07	0.06	<d.l.[a]
K_2O	<d.l.[a]	<d.l.[a]	0.12	0.12	<d.l.[a]
Na_2O	0.06	0.14	<d.l.[a]	<d.l.[a]	0.07
P_2O_5	0.02	<d.l.[a]	<d.l.[a]	<d.l.[a]	0.02

[a]Concentrations were below detection limit.

Table 3 – Grey and ferruginous chert major element geochemistry, weight %, normalized to 100% on a volatile-free basis

Sample	**SAF 518-15**	**SAF 518-30**	**SAF 186-65**	**SAF 186-66**	**SAF 186-67**	**SAF 521-12**	**SAF 483-9**
Source	This study	This study	This study	This study	This study	This study	This study
Formation	Mendon	Mendon	Mendon	Mendon	Mendon	Fig Tree	Mendon
Lithology	Lam. grey	Lam. grey	BFC	BFC	BFC	Lam. ferr.	White silicified sed.
SiO_2	90.89	96.37	95.55	91.75	90.58	95.62	95.06
Al_2O_3	2.35	2.54	1.08	2.53	0.50	0.82	3.02
TiO_2	0.08	0.09	0.02	0.05	0.01	0.03	0.10
FeO*	5.90	0.18	2.83	4.46	6.36	2.34	0.61
MnO	0.04	<d.l.[a]	0.09	0.09	0.52	0.09	<d.l.[a]
CaO	0.11	0.10	0.35	0.01	0.18	0.91	0.20
MgO	<d.l.[a]	0.01	<d.l.[a]	0.98	1.76	0.02	0.30
K_2O	0.01	<d.l.[a]	0.00	0.07	0.03	<d.l.[a]	0.59
Na_2O	0.59	0.69	0.07	0.03	0.05	0.15	0.10
P_2O_5	0.03	0.01	0.01	<d.l.[a]	0.02	0.02	0.02

[a]Concentrations were below detection limit.

Table 4 – Trace element geochemistry (ppm) determined by XRF

Sample	SAF 199-10	SAF 521-3	SAF 521-10	SAF 483-1	SAF 518-15	SAF 518-30	SAF 186-65	SAF 186-66	SAF 186-67	SAF 521-12
Formation	Mendon	Mendon	Fig Tree	Mendon	Mendon	Mendon	Mendon	Mendon	Mendon	Fig Tree
Lithology	BBWC	BBWC	BBWC	Lam. BC	Lam. grey	Lam. grey	BFC	BFC	BFC	Lam. ferr.
Ni	34	12	23	225	62	7	50	84	61	55
Cr	33	20	121	134	69	73	24	23	16	46
Sc	0	0	1	0	6	2	0	6	6	2
V	6	6	13	9	19	18	6	10	1	11
Ba	26	181	679	823	2609	1555	33	30	54	405
Rb	2	3	6	5	21	27	2	3	2	6
Sr	3	2	19	7	3	2	2	4	6	1
Zr	8	6	12	6	16	19	12	31	9	11
Y	1	1	2	1	5	7	8	12	6	3
Nb	0.2	0.2	0.9	2.0	0.4	1.0	0.7	4.5	3.1	1.6
Ga	0	0	1	2	4	4	3	6	0	2
Cu	2	3	8	34	25	0	21	0	4	22
Zn	5	3	3	2	3	0	12	4	2	4
Pb	0	1	0	34	3	4	1	4	0	2
La	0	0	0	16	11	6	3	3	0	0
Ce	7	4	5	12	8	13	6	26	6	5
Th	0	1	1	0	0	2	0	4	0	0

Table 5 – Rare earth element ratios

Sample Lithology	SAF-521-3 BBWC	SAF-521-10 BBWC	SAF-199-10 BBWC	SAF 518-15 Lam. grey	SAF 518-30 Lam. grey	SAF-521-12 Lam. ferr.	SAF 186-65 BFC	SAF-186-67 BFC	SAF-186-62 Silicified ash
Y/Ho	*34.64*	*34.61*	*31.61*	25.27	*29.62*	*34.85*	*27.58*	*30.27*	*28.88*
La/La*[a]	*1.41*	*1.52*	*1.53*	*1.02*	*1.09*	*1.61*	*1.21*	*1.54*	*1.30*
Gd/Gd*[a]	*1.05*	*1.12*	*1.05*	1.00	*1.12*	*1.19*	*1.19*	*1.17*	*1.11*
Gd_{SN}/Yb_{SN}[b]	*0.79*	*0.97*	*0.74*	*0.99*	*0.57*	*0.88*	*0.70*	*0.56*	1.94
La_{SN}/Yb_{SN}[b]	*0.61*	*0.85*	1.05	1.67	*0.69*	*0.54*	*0.38*	*0.29*	2.26
Ce/Ce*[a]	*1.11*	*1.13*	*1.05*	0.41	*0.98*	*1.17*	*1.02*	*1.11*	0.59
Eu/Eu*[c]	*1.18*	*0.97*	*1.12*	*0.82*	*0.87*	*1.00*	*0.97*	1.40	*0.78*

Italicized values pass the criterion of Bolhar et al. (2004) for originating from seawater, summarized in text. Although not discussed in detail by Bolhar et al. (2004), most Ce and Eu anomalies are also consistent with an Archean seawater signal.

[a]Ratios calculated as in Bolhar et al. (2004).

[b]Ratios of abundances normalized to PAAS shale standard (SN) (Taylor and McLennan, 1985).

[c]Ratios of abundances normalized to chondrite (Taylor and McLennan, 1985).

Highlights

- Hemipelagic settling of organic matter was the dominant mode of sedimentation.
- Background deposition was punctuated by volcanic inputs and storm deposits.
- Oldest Mendon sections record upward-deepening, consistent with rifting hypothesis.
- Higher Mendon cycles reflect gradual shoaling.

Figure 1

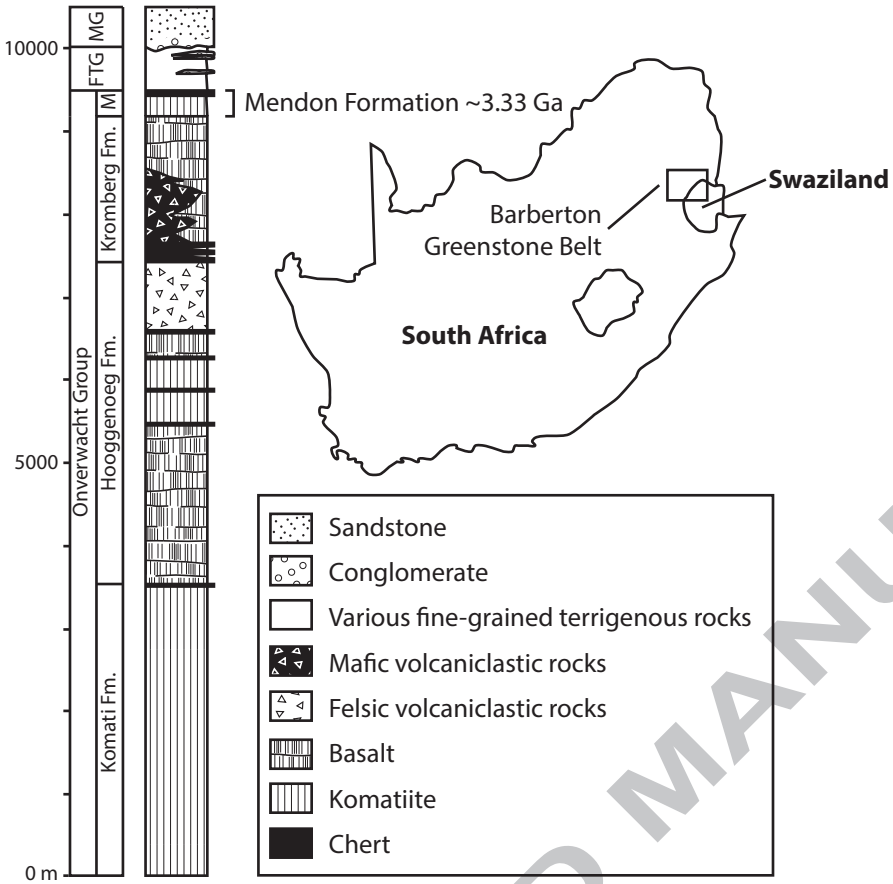

Figure 2

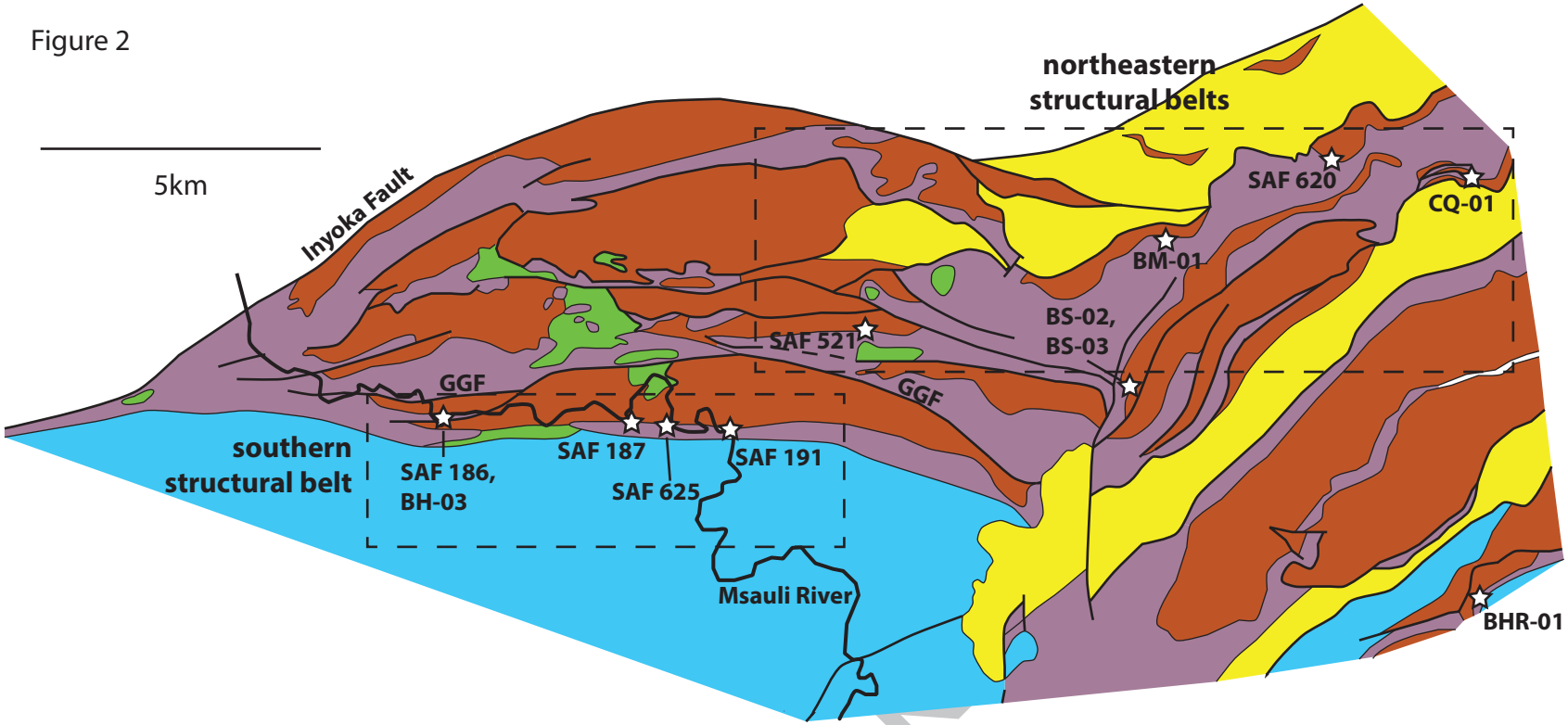

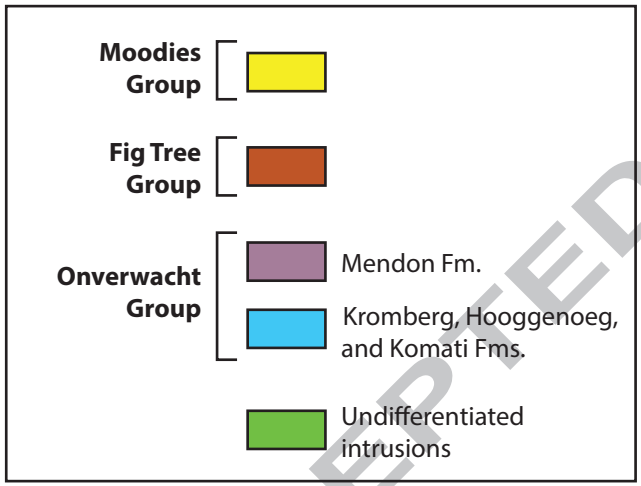

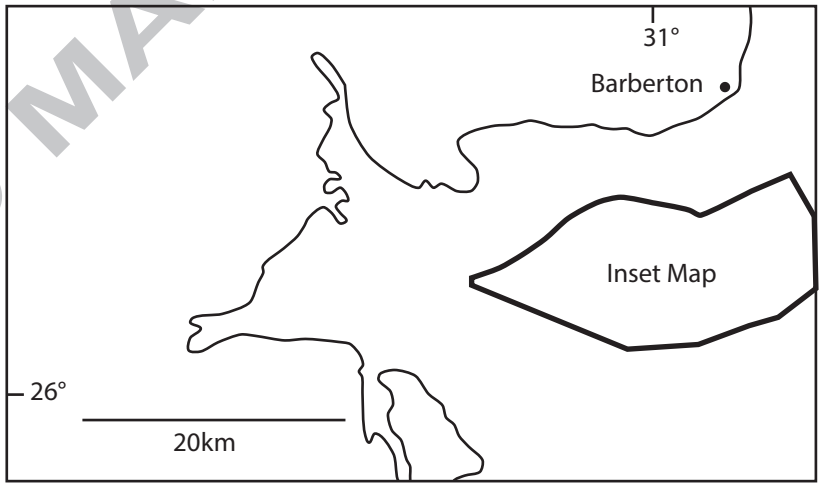

Figure 3

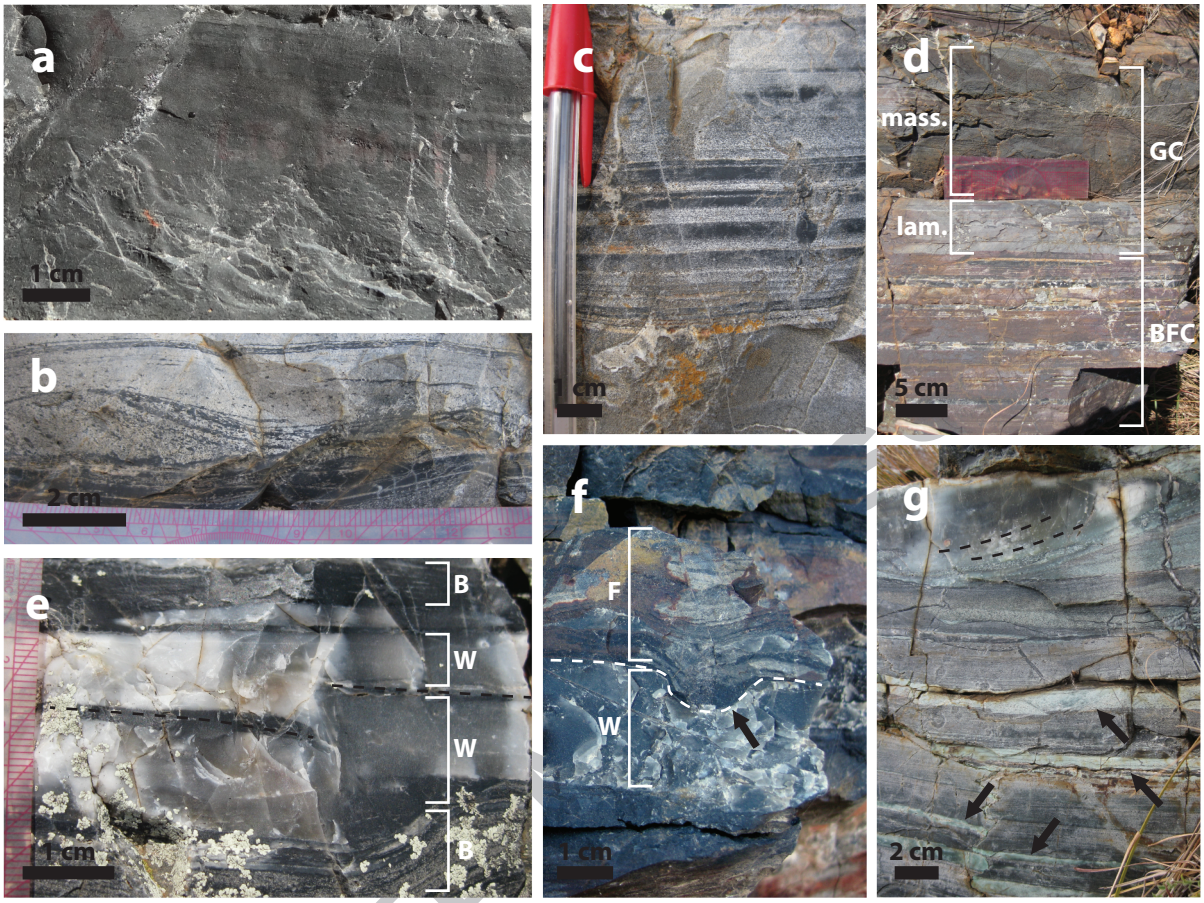

Figure 4

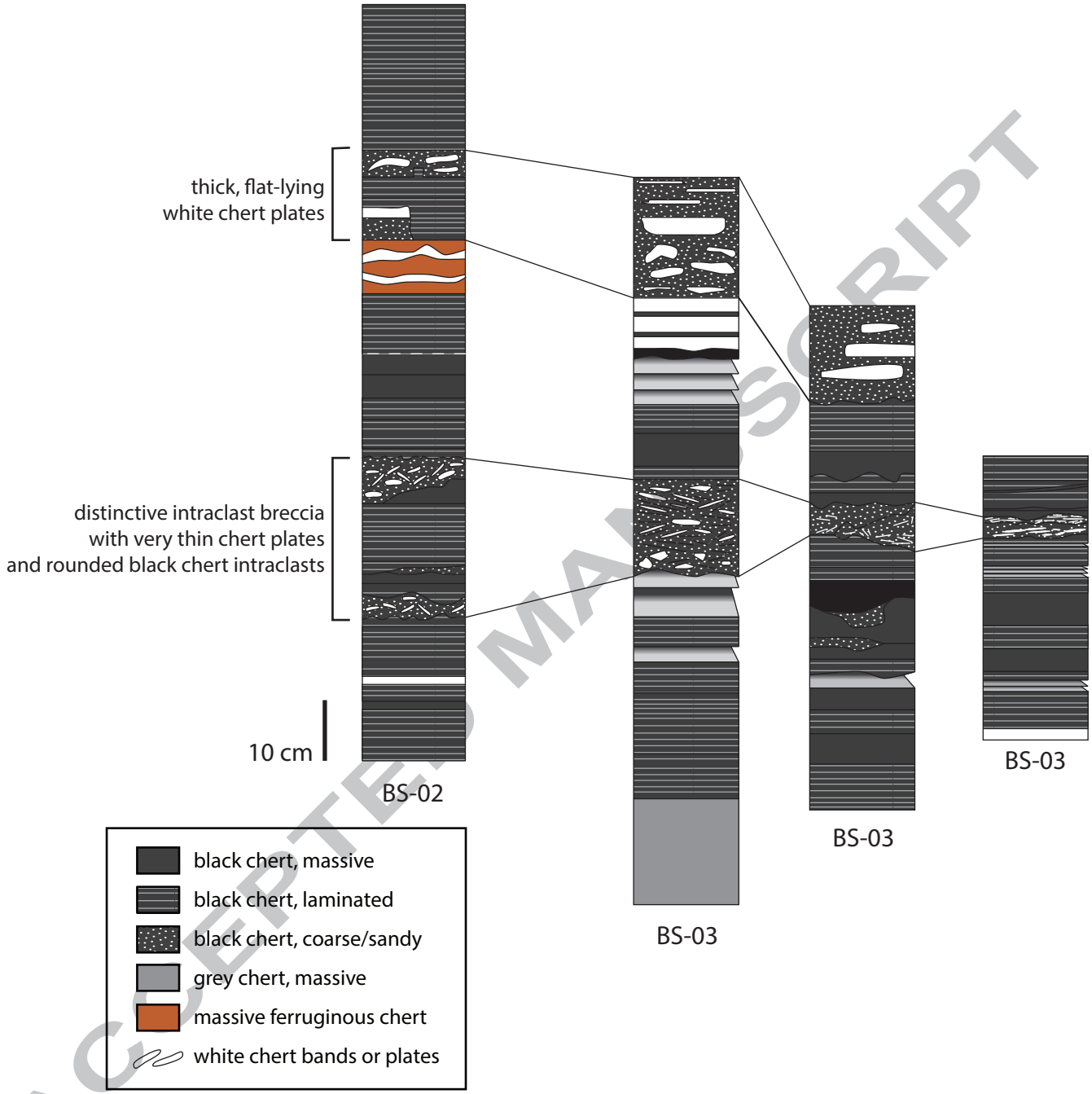

Figure 5

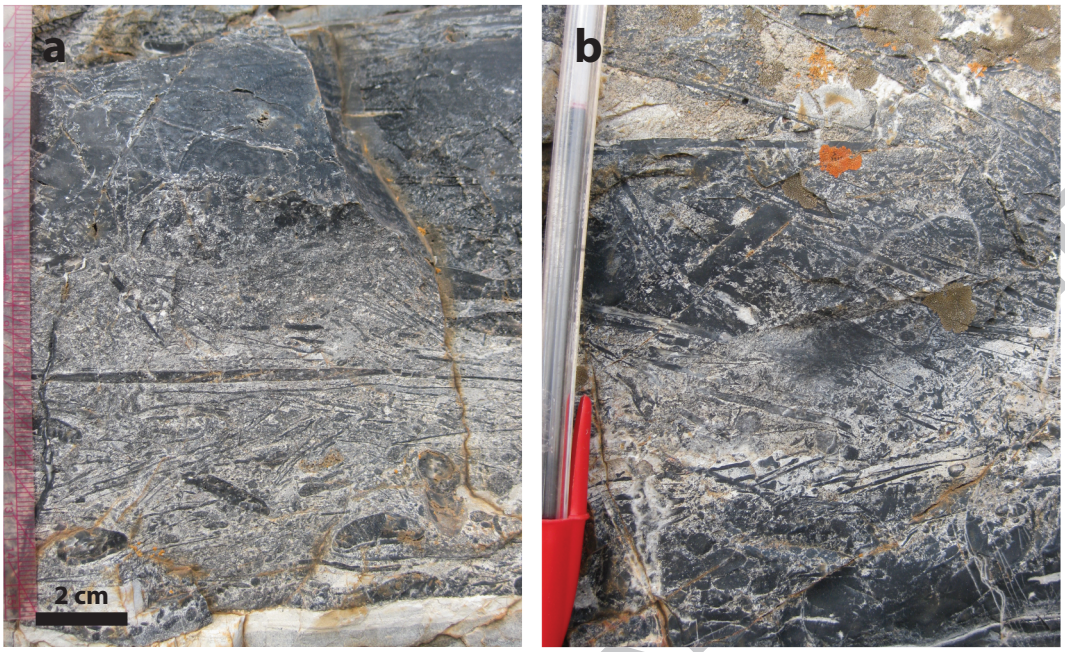

Figure 6

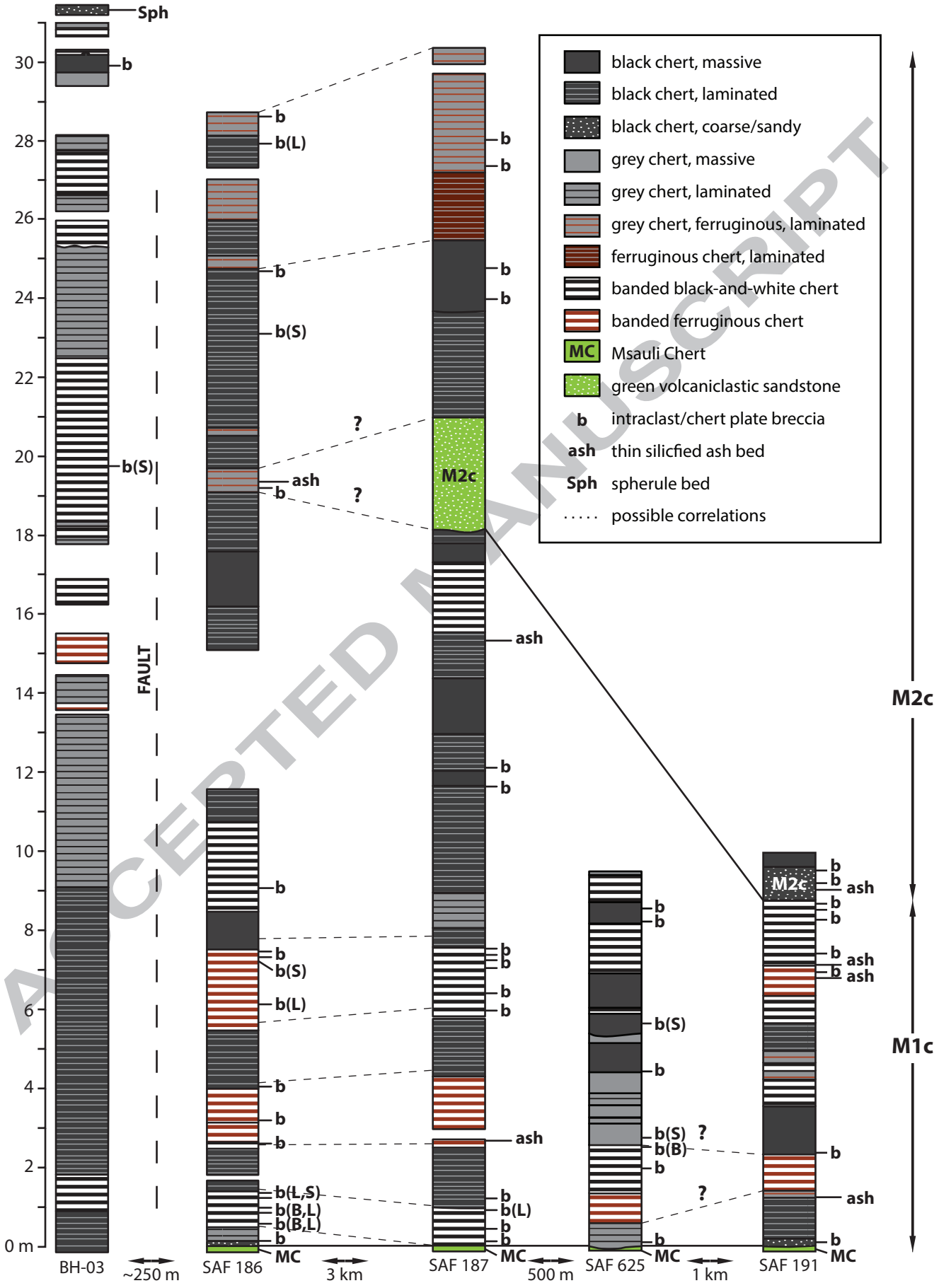

Figure 7

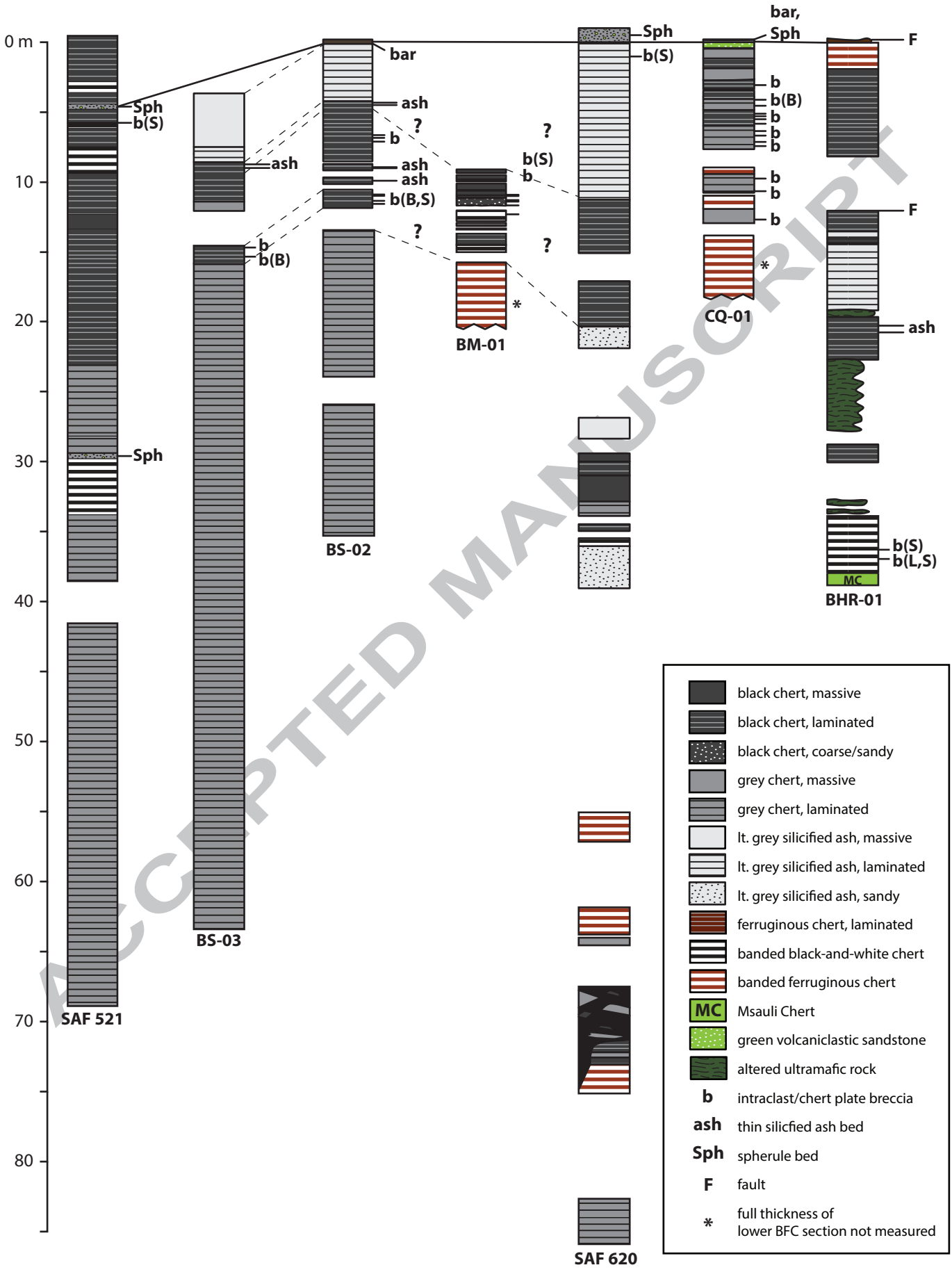

Figure 8

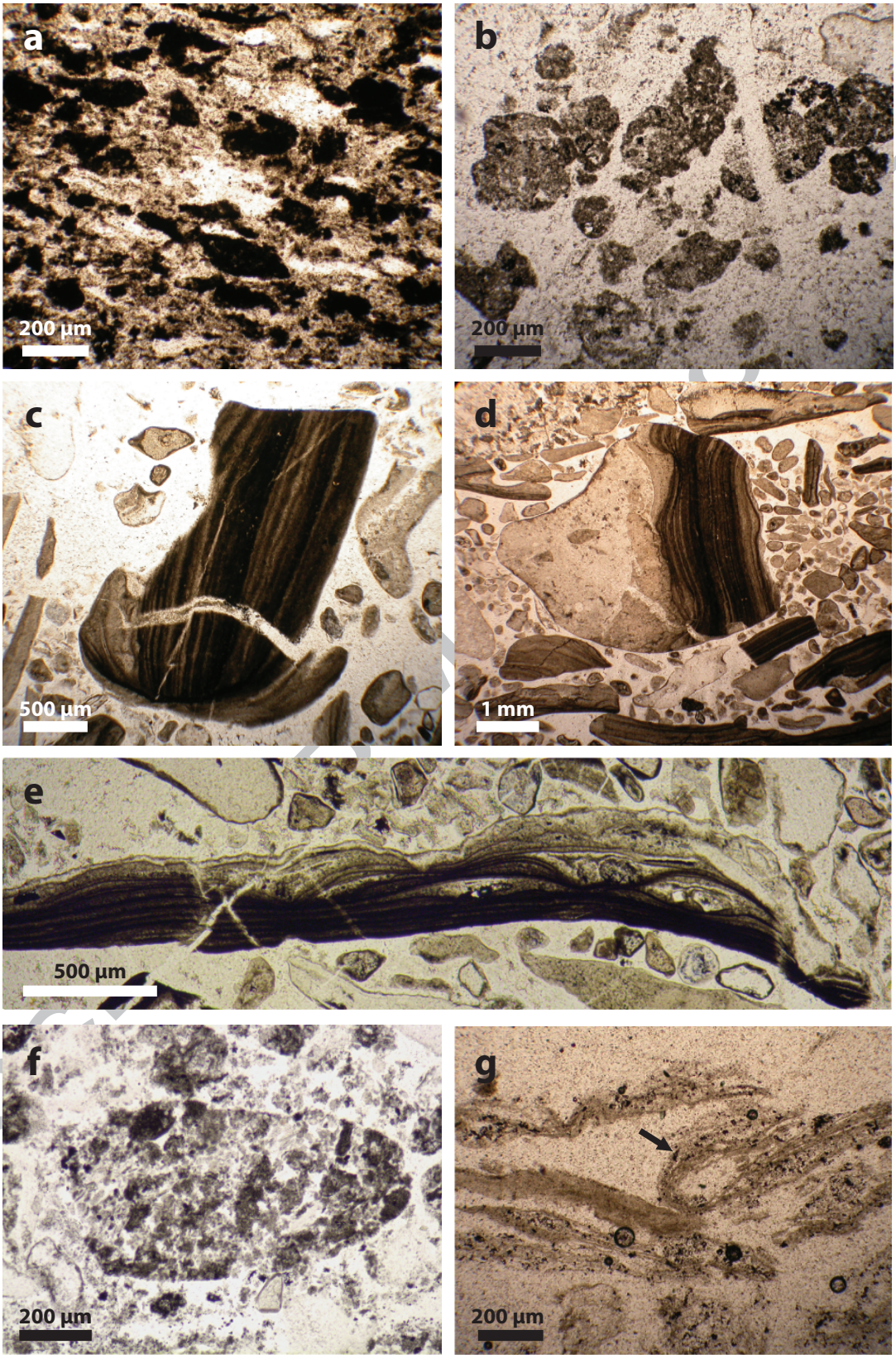

Figure 9

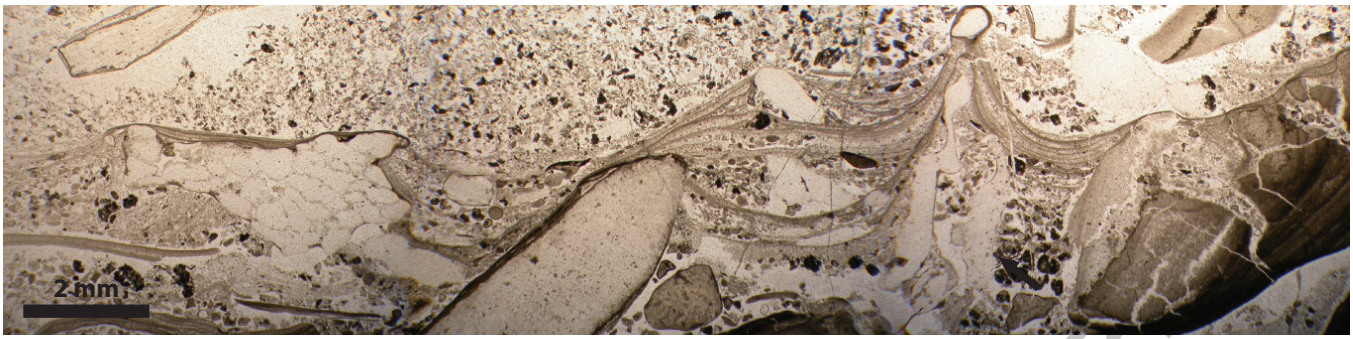

Figure 10

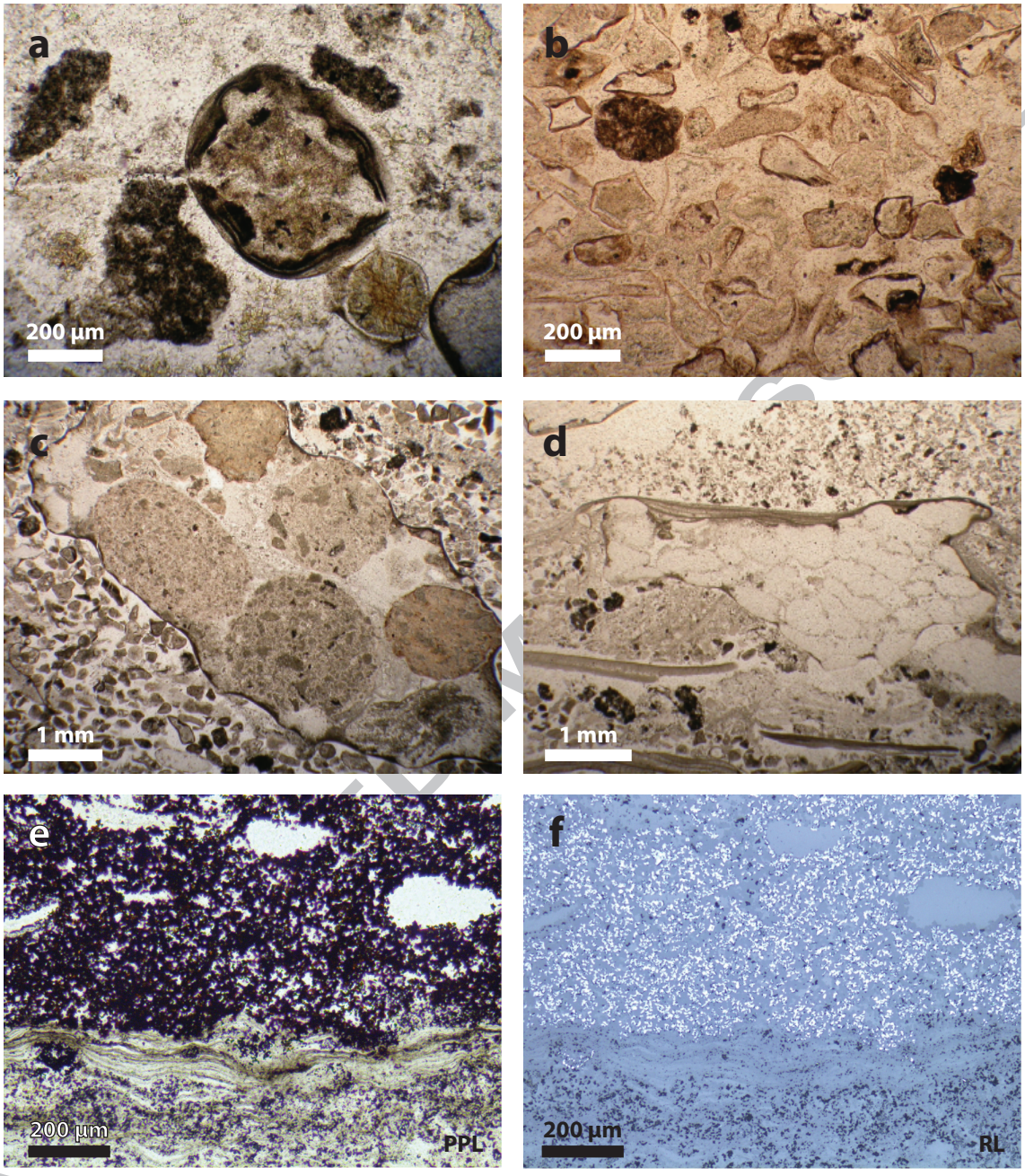

Figure 11

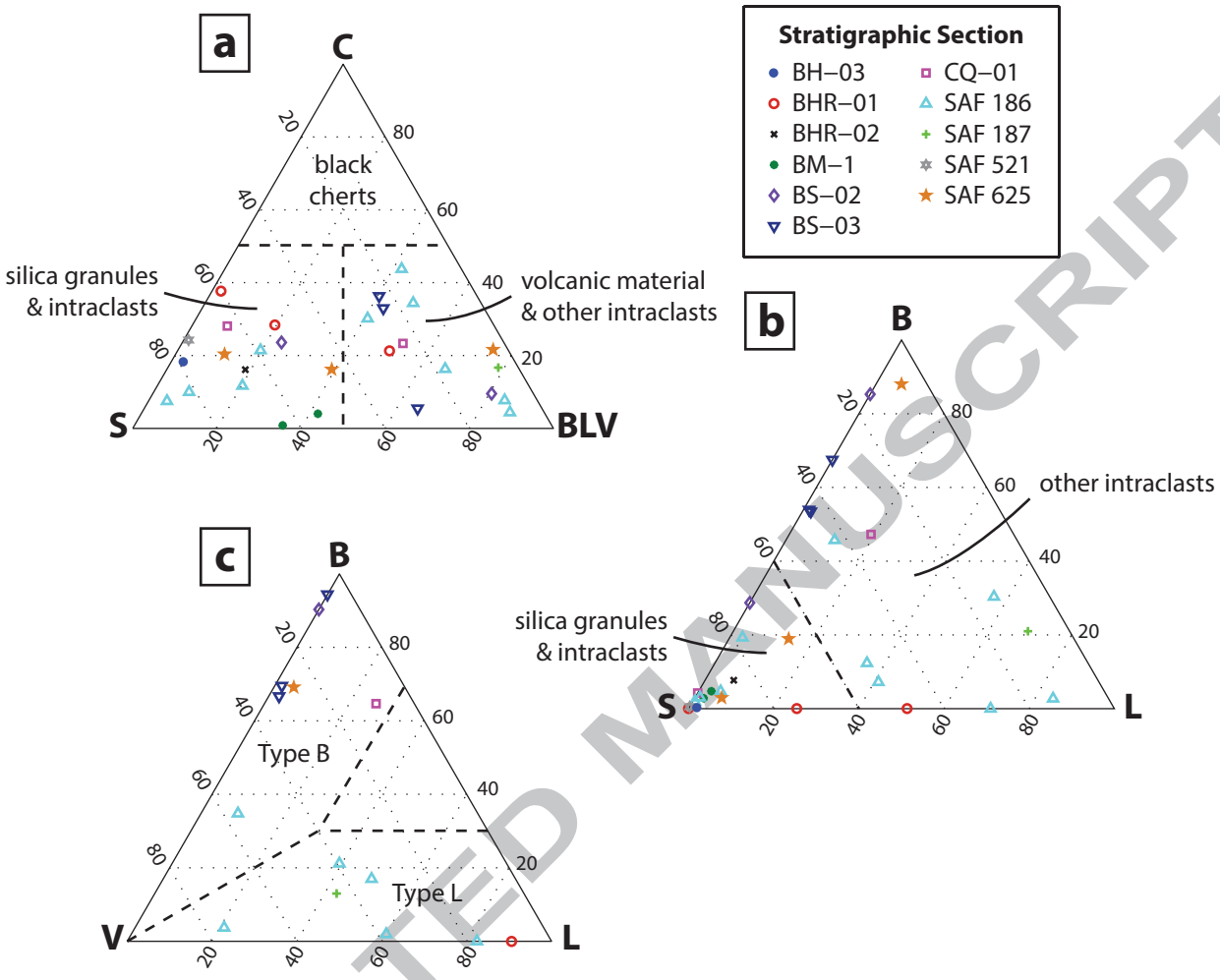

Figure 12

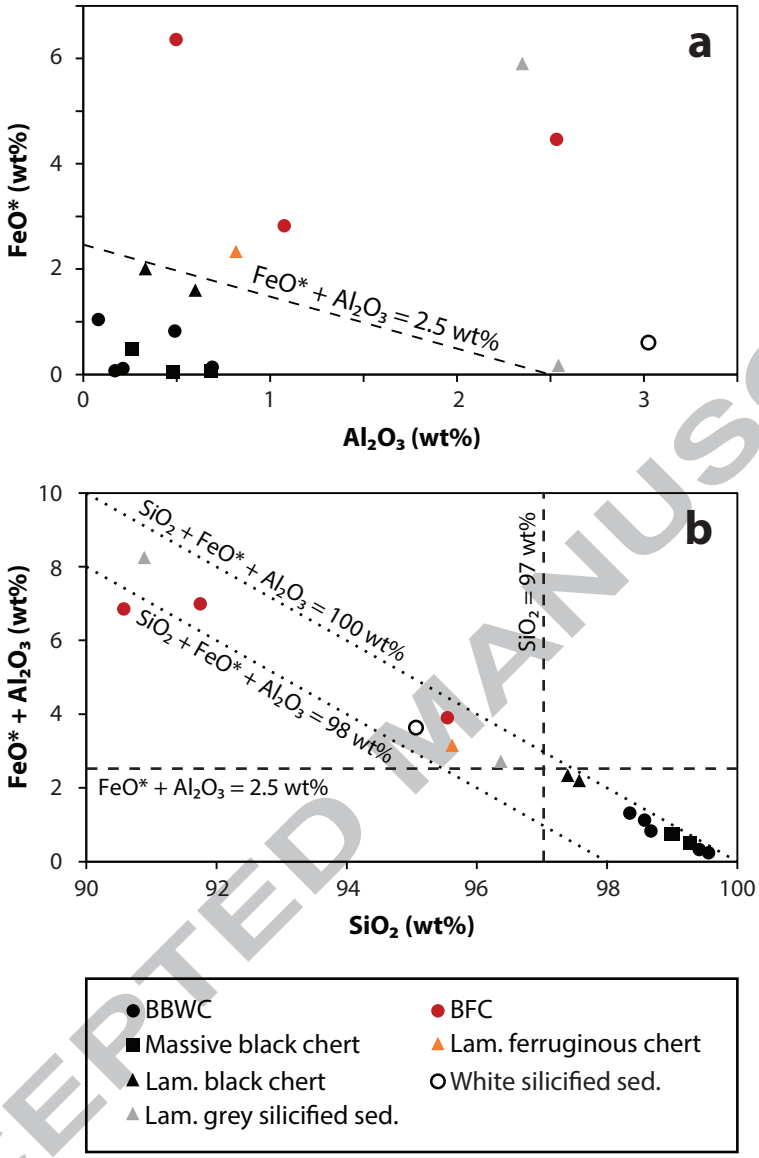

Figure 13

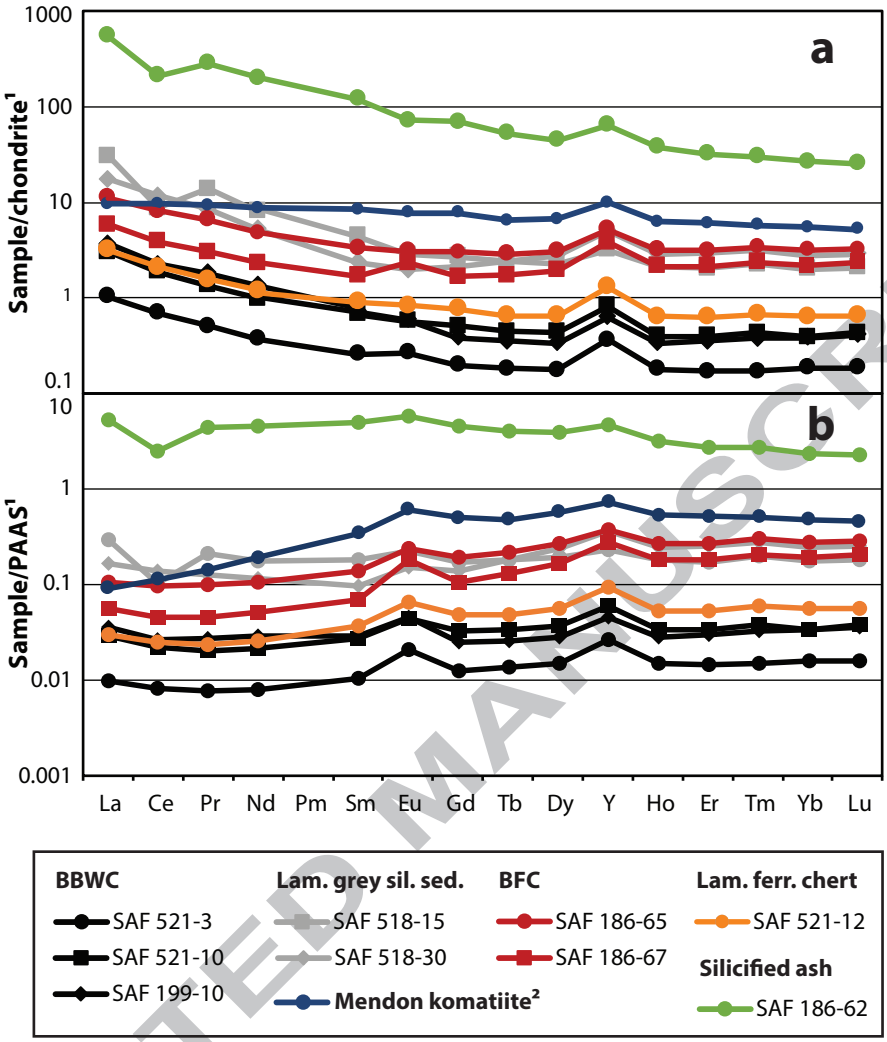

Figure 14

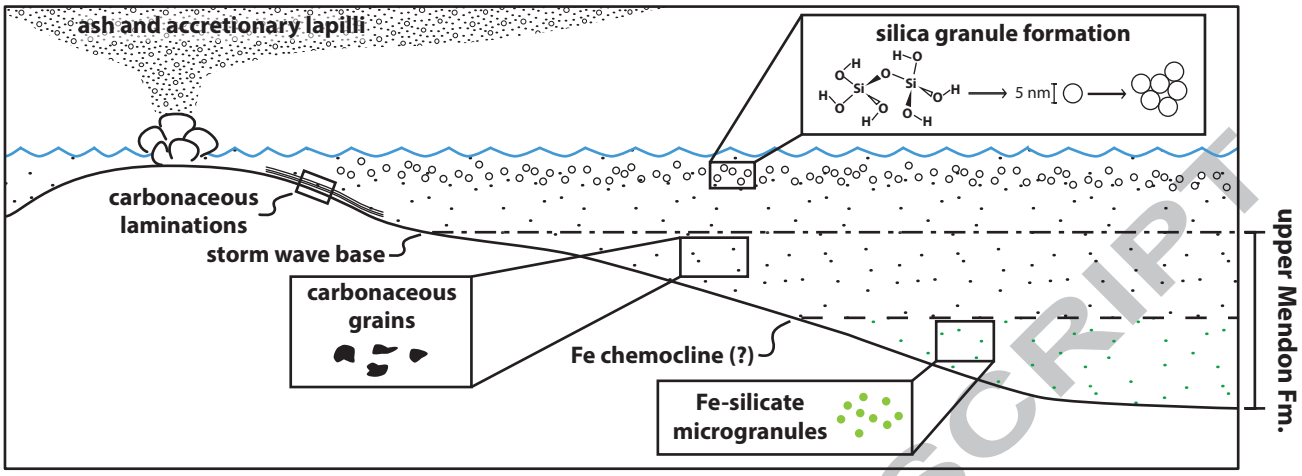

Figure 15

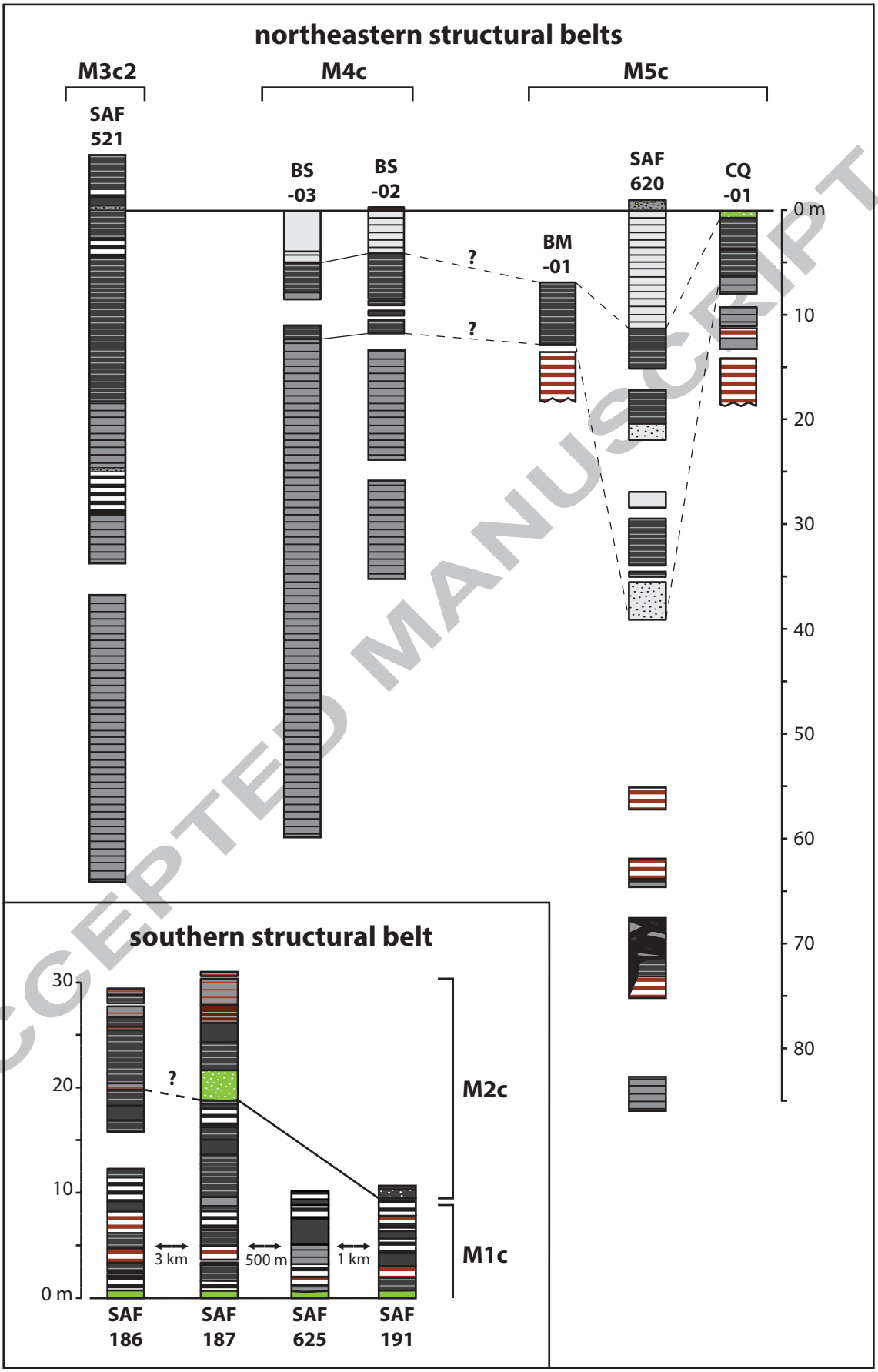

Figure 16